Spin squeezing of a Bose-Einstein condensate via a quantum nondemolition measurement for quantum-enhanced atom interferometry

Michail Kritsotakis,[1,*] Jacob A. Dunningham [ORCID],[1] and Simon A. Haine[2]

[1]*Department of Physics and Astronomy, University of Sussex, Brighton BN1 9QH, United Kingdom*
[2]*Department of Quantum Science, Research School of Physics and Engineering, The Australian National University, Canberra, Australian Capital Territory 2601, Australia*

We theoretically investigate the use of quantum nondemolition measurement to enhance the sensitivity of atom interferometry with Bose-condensed atoms. In particular, we are concerned with enhancing existing high-precision atom interferometry apparatuses, and so restrict ourselves to dilute atomic samples and the use of free-propagating light or optical cavities in the weak-coupling regime. We find the optimum parameter regime that balances between spin squeezing and atomic loss and find that significant improvements in sensitivity are possible. Finally, we consider the use of squeezed light and show that this can provide further boosts to sensitivity.

I. INTRODUCTION

Atom interferometers are powerful tools for making precision measurements particularly in the realm of inertial navigation since they can provide sensitive measurements of accelerations and rotations with very low baseline drift [1,2]. A lot of interest has therefore developed in finding ways of improving their performance to gain advantage in different applications. It has been shown that Bose-condensed atomic sources can outperform thermal sources due to their narrow momentum linewidth, despite their reduced atomic flux [3–7]. The use of nonclassical atomic states such as spin-squeezed states can offset this reduction in flux even further by allowing for sensitivities beyond the shot-noise limit (SNL) [8–11]. In this paper, we investigate the use of quantum nondemolition (QND) measurements in collections of Bose-condensed atoms to generate quantum states that could be used to enhance their precision in a range of metrology schemes. The mechanism for generating quantum enhanced many-atom states can be broadly classified into two categories: Those that use atom-atom interactions [9,12–19] and those that use atom-light interactions [20–38]. While several experiments have demonstrated nonclassical states generated through atom-atom interactions [39–48], so far these have been restricted to small numbers of atoms and have not been applied to atom interferometry capable of inertial measurements. This is partly because the atom-atom interactions required for the generation of the entanglement create unavoidable multimode dynamics which inhibit mode matching [18,49–52] and phase diffusion [53,54]. Quantum entanglement through atom-light interactions, which are free to operate in regimes where the effects of atom-atom interactions are negligible, have also been successfully demonstrated. In particular, the use of light to perform QND measurements of the collective atomic spin has shown significant spin squeezing [55–63]. So far, these

experimental demonstrations have been restricted to cold thermal atoms. In this work, we focus on Bose-condensed sources, with the motivation of implementing this quantum enhancement technique on existing high-precision, large space-time area atomic gravimetry setups, such as in Ref. [64]. In particular, the requirement that the Bose-Einstein condensate (BEC) is expanded before the atomic beam-splitting process dictates a minimum spatial size of the source and prevents excessively elongated samples, such as in Ref. [61]. Furthermore, we restrict ourselves to freely propagating light and find the optimum parameter regime which balances the spin squeezing and atomic loss caused by spontaneous emission. We also consider the use of optical cavities but restrict ourselves to cavities that are assembled outside the vacuum chamber, which are inherently low finesse with weak atom-light coupling due to the large cavity volume. We also consider the use of squeezed light to further enhance the sensitivity.

This paper is structured as follows. In Sec. II, we review atom interferometry and quantify how spin squeezing via QND measurements improves the sensitivity. In Sec. III, we introduce a simple model of QND squeezing which allows us to make some simple analytic scaling predictions. In Sec. IV we present our full model including a freely propagating multimode optical field and decoherence due to spontaneous emission. In Sec. V, we derive approximate analytic solutions to this model, and in Sec. VI we analyze the system numerically. In Sec. VII, we examine the effect of BEC interactions on the level of spin squeezing. In Sec. VIII, we investigate how the use of squeezed light affects the behavior. In Sec. IX, we investigate the use of an optical cavity.

II. USING QND MEASUREMENTS TO ENHANCE THE SENSITIVITY OF A MACH-ZEHNDER INTERFEROMETER

Atom interferometers used to measure accelerations and rotations are usually based on the Mach-Zehnder (MZ) configuration [65,66]. Starting with an ensemble of atoms with

---

*M.Kritsotakis@sussex.ac.uk

023318-1

two stable ground states, labeled $|1\rangle$ and $|2\rangle$, a $\frac{\pi}{2}$ pulse, or beam splitter, implemented by a two-photon Raman transition is used to place each atom in an equal superposition of these states, while transferring momentum $\hbar\mathbf{k}_0$ to the state $|2\rangle$ component, where $\mathbf{k}_0$ is determined by the difference in wave vectors of the two Raman lasers. The atoms then evolve for a period of time T before a second Raman transition implements a π pulse, or "mirror." After a second period of time T, a second $\frac{\pi}{2}$ beam-splitter pulse is implemented, and the number difference is read out. Such a system is conveniently described by introducing the pseudospin operators $\hat{J}_k$ defined by

$$\hat{J}_k = \frac{1}{2}(\hat{a}^\dagger, \hat{b}^\dagger)\sigma_k\begin{pmatrix}\hat{a}\\\hat{b}\end{pmatrix},\tag{1}$$

with $k = x, y, z$, where σ_k is the kth Pauli matrix and $\hat{a}, \hat{b}$ are the annihilation operators of a particle from $|a\rangle$ and $|b\rangle$ modes respectively. These operators obey the SU(2) commutation relations

$$[\hat{J}_x, \hat{J}_y] = i\hat{J}_z, \ [\hat{J}_y, \hat{J}_z] = i\hat{J}_x, \ [\hat{J}_z, \hat{J}_x] = i\hat{J}_y.\tag{2}$$

It can be shown that the MZ interferometer described above performs the operation

$$\hat{J}_k = e^{i\hat{J}_y\theta}\hat{J}_k(0)e^{-i\hat{J}_y\theta},\tag{3}$$

where θ is the phase difference that has accumulated between the two arms of the interferometer and $\hat{J}_k(0)$ are the operators before the pulse sequence [7,67–69]. For a gravimeter, $\theta = \mathbf{g}\cdot\mathbf{k}_0 T^2$, where $\mathbf{g}$ is the gravitational field. The task of estimating g, the magnitude of the gravitational field parallel to $\mathbf{k}_0$, then comes down to our ability to estimate θ. That is, $\Delta g = \Delta\theta/|\mathbf{k}_0|T^2$.

For a particular measurement signal $\hat{S}$, the sensitivity is given by

$$\Delta\theta = \sqrt{\frac{\mathrm{Var}(\hat{S})}{(\partial_\theta\langle\hat{S}\rangle)^2}}.\tag{4}$$

Choosing $\hat{S}_1 = \hat{J}_z$ for $\hat{S}$, the number difference at the output of the interferometer, we find

$$\hat{J}_z = \hat{J}_z(0)\cos(\theta) - \hat{J}_x(0)\sin(\theta).\tag{5}$$

Operating around $\theta \approx 0$, we find

$$\Delta\theta = \sqrt{\frac{\mathrm{Var}(\hat{J}_z)}{(\langle\hat{J}_x\rangle)^2}}.\tag{6}$$

Choosing an initial state as N_a uncorrelated atoms in an equal superposition of $|1\rangle$ and $|2\rangle$, i.e., a coherent spin state [70],

$$|\Psi\rangle = \left[\frac{1}{\sqrt{2}}(\hat{a}^\dagger + \hat{b}^\dagger)\right]^{\otimes N_a}|0,0\rangle,\tag{7}$$

we find

$$\Delta\theta = \frac{1}{\sqrt{N_a}},\tag{8}$$

which is the shot-noise limit (SNL). This is the best possible sensitivity for any uncorrelated state. That is, any state of

the form $|\Psi\rangle = (c_1|1\rangle + c_2|2\rangle)^{\otimes N_a}$. Equation (8) motivates the introduction of the spin-squeezing parameter ξ_s, defined by

$$\xi_s = \sqrt{N_a}\frac{\sqrt{\mathrm{Var}(\hat{S})}}{|\partial_\theta\langle\hat{S}\rangle|}\tag{9}$$

such that

$$\Delta\theta = \frac{\xi_s}{\sqrt{N_a}}.\tag{10}$$

The use of input states with quantum correlations such that $\xi_s < 1$ gives sensitivities better than the SNL. We should point out here that we consider a scheme where the preparation of the entanglement-enhanced state and the interferometer sequence are two completely separate stages of the whole procedure. Essentially, we first prepare a spin-squeezed state, which would be used as the input state of the interferometer. This is the reason why we will explicitly denote in the following that $\theta = 0$ in the atomic variables, which is the point of interest, since in practice the interferometer is biased to operate around the most sensitive point, which is $\theta = 0$. A state with $\xi_s < 1$ can be achieved by creating atom-atom entanglement and also by creating entanglement between the atoms and some auxiliary field, such as an optical beam. By measuring both fields together, it is possible to create a signal with reduced fluctuations and therefore increased sensitivity, specifically, by measuring the combined signal

$$\hat{S}_2 = \hat{J}_z(0) - \hat{J}_z^{\mathrm{inf}},\tag{11}$$

where $\hat{J}_z^{\mathrm{inf}} = G\hat{S}_b$ represents an inference of the population difference, based on measurements of some optical observable $\hat{S}_b$. The constant G is a proportionality factor, which is found by minimizing the variance of the total signal $\mathrm{Var}(\hat{S}_2)$ with respect to G,

$$G = \frac{\mathrm{Cov}(\hat{J}_z(0), \hat{S}_b)}{\mathrm{Var}(\hat{S}_b)},\tag{12}$$

which gives

$$\mathrm{Var}(\hat{S}_2) = \mathrm{Var}(\hat{J}_z(0)) - \frac{\mathrm{Cov}^2(\hat{J}_z, \hat{S}_b)}{\mathrm{Var}(\hat{S}_b)}.\tag{13}$$

Hence, creating atom-light entanglement and measuring the appropriate light observable in such a way that $\frac{\mathrm{Cov}^2(\hat{J}_z(0), \hat{S}_b)}{\mathrm{Var}(\hat{S}_b)} > 0$ yields a reduced signal variance $\mathrm{Var}(\hat{S}_2) < \mathrm{Var}(\hat{J}_z(0)) = \mathrm{Var}(\hat{S}_1)$, increasing the sensitivity over purely measuring the population difference between the two interferometer modes. As the optical observables are unaffected by the MZ sequence, which only acts on atomic degrees of freedom, at $\theta = 0$ we have $\Delta\theta = \xi_{s_2}/\sqrt{N_a}$, where

$$\xi_{s_2} = \frac{\sqrt{N_a}\sqrt{\mathrm{Var}(\hat{S}_2)}}{|\langle\hat{J}_x\rangle|}.\tag{14}$$

Hence, if we use an atomic state with $\xi_{s_2} < 1$ as the input state of the interferometer it would result in a performance surpassing the SNL ($\Delta\theta < 1/\sqrt{N}$). If the Hamiltonian responsible for the atom-light entanglement commutes with $\hat{J}_z$, then this is an example of a QND measurement, as there is no measurement backaction on the observable being measured. In the
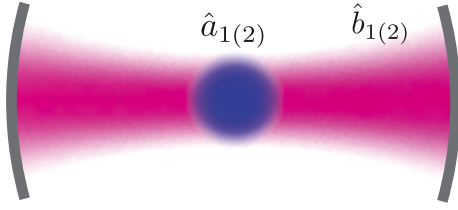
FIG. 1. Simplified scheme showing QND entanglement via an atom-light interaction. An optical mode represented by annihilation operator $\hat{b}_{1(2)}$ interacts with an ensemble of Bose-condensed atoms (annihilation operator $\hat{a}_{1(2)}$).

next section, we model the atom-light interaction and quantify how the appropriate choice of $\hat{S}_b$ improves the sensitivity.

III. SIMPLE MODEL: SINGLE-MODE LIGHT FIELDS

In order to demonstrate how QND squeezing affects the sensitivity, we begin with a simplified model where we make the single-mode approximation for both the atomic fields and optical fields, sssuming an ensemble of two-level atoms in the ground motional state of a trapped BEC, with each level interacting with a far-detuned laser beam, as described in Fig. 1.

The simplified Hamiltonian for the system is

$$\hat{H}_{\text{int}} = -\hbar\chi_{\text{sm}}(\hat{a}_1^\dagger\hat{a}_1\hat{b}_1^\dagger\hat{b}_1 + \hat{a}_2^\dagger\hat{a}_2\hat{b}_2^\dagger\hat{b}_2), \tag{15}$$

where χ_{sm} indicates the interaction strength between the atoms and the light in our simple model. Also, $\hat{a}_j = \int u_0^*(\mathbf{r})\hat{\psi}_j(\mathbf{r})\,d^3\mathbf{r}$ annihilates an atom from the ground motional state of the BEC [spatial wave function $u_0(\mathbf{r})$], and $\hat{b}_j$ annihilates a photon from the optical mode interacting with atomic state $|j\rangle$. The atomic and light operators satisfy $[\hat{a}_i, \hat{a}_j^\dagger] = \delta_{ij}$ and $[\hat{b}_i, \hat{b}_j^\dagger] = \delta_{ij}$ respectively. As both $\hat{a}_j^\dagger\hat{a}_j$ and $\hat{b}_j^\dagger\hat{b}_j$ commute with the Hamiltonian, the solution to the Heisenberg equations of motion for the system are

$$\hat{a}_j(t) = \hat{a}_j(0)e^{i\chi_{\text{sm}}\hat{b}_j^\dagger(0)\hat{b}_j(0)t}, \tag{16a}$$

$$\hat{b}_j(t) = \hat{b}_j(0)e^{i\chi_{\text{sm}}\hat{a}_j^\dagger(0)\hat{a}_j(0)t}. \tag{16b}$$

Examining the form of Eq. (16b), we see that the phase of the optical mode is correlated with the population of the corresponding atomic mode. This motivates us to examine $\hat{Y}_{b_j}$, where $\hat{Y}_{b_j} = i(\hat{b}_j - \hat{b}_j^\dagger)$ is the phase quadrature of the light field. After making the small angle approximation $\chi_{\text{sm}}t\hat{a}_j^\dagger\hat{a}_j \ll 1$ we find

$$\hat{Y}_j(t) \approx \hat{Y}_{j0} - \chi_{\text{sm}}t\hat{a}_j^\dagger\hat{a}_j\hat{X}_{j0} \tag{17}$$

where $\hat{Y}_{j0} = i(\hat{b}_j(0) - \hat{b}_j^\dagger(0))$ and $\hat{X}_{j0} = \hat{b}_j(0) + \hat{b}_j^\dagger(0)$, and notice that $\hat{Y}_j(t) \propto \hat{N}_{a_j}$. Hence we can make an inference about the atomic population difference by measuring the difference of the two phase quadratures. In order to calculate the strength of these correlations, we choose Glauber coherent states $|\alpha_j\rangle$ and $|\beta_j\rangle$, with $\text{Im}(\alpha_j) = \text{Im}(\beta_j) = 0$ as the initial state for the atomic and optical modes respectively. This corresponds to an atomic state with the expectation value of the spin aligned to the x-axis, but with a fluctuating total number. The choice of a Glauber coherent state rather than a
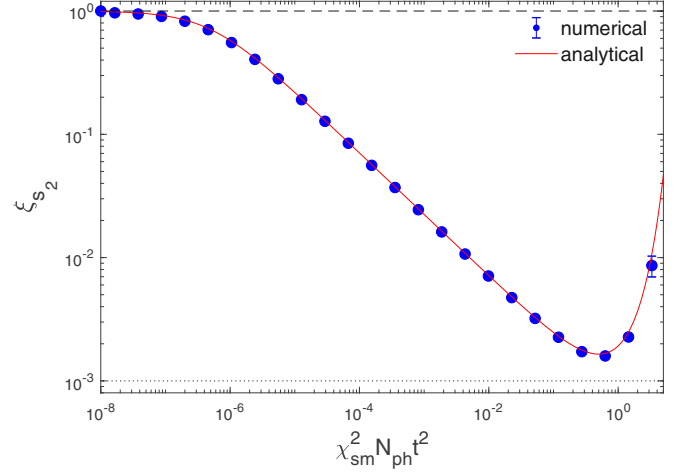

FIG. 2. Simple model: Analytical (red solid line) and numerical calculation (blue dots) of ξ_{s_2} with respect to the collective parameter $\chi_{\text{sm}}^2 N_{\text{ph}} t^2$. The black dashed and dotted lines represent the SNL and the Heisenberg limit respectively. The error bars were calculated by taking the standard deviation over many different iterations of the system dynamics.

coherent spin state was for computational convenience. It has previously been shown that for large atom number, this state provides almost identical spin-squeezing predictions [71]. As there is no physical process that couples parts of the Hilbert space corresponding to different values of the *total* atom number, whether this state is a true number superposition, or an incoherent mixture of total atom number has no observable consequence [49]. This state can be obtained by beginning with all the atoms in one state, and applying a rotation around the y-axis (i.e. and atomic beamsplitter). Setting $\hat{S}_b = \hat{Y}_2 - \hat{Y}_1$ we find

$$\text{Var}(\hat{S}_b(t)) \approx 2 + 4\chi_{\text{sm}}^2 N_{\text{ph}} N_a t^2, \tag{18}$$

and

$$\text{Var}(\hat{S}_2(t)) = \frac{N_a}{4}\left(1 - \frac{2\chi_{\text{sm}}^2 N_a N_{\text{ph}} t^2}{1 + 2\chi_{\text{sm}}^2 N_a N_{\text{ph}} t^2}\right) \tag{19}$$

where $N_{\text{ph}} = |\beta_1|^2 = |\beta_2|^2$ is the expectation value of the number of photons. Using this in Eq. (14) we find

$$\xi_{s_2} = e^{\chi_{\text{sm}}^2 N_{\text{ph}} t^2}\left(1 - \frac{2\chi_{\text{sm}}^2 N_a N_{\text{ph}} t^2}{1 + 2\chi_{\text{sm}}^2 N_a N_{\text{ph}} t^2}\right)^{1/2}. \tag{20}$$

We notice in Fig. 2 that we obtain better sensitivities for our signal compared to the SNL, indicating that we have created a spin squeezed state. We find the optimum value for the number of photons $N_{\text{ph}}^{\text{opt}} = \frac{1}{2\chi_{\text{sm}}^2 t^2}$ which gives the minimum value $(\xi_{s_2}^{\text{sm}})_{\text{min}} = \sqrt{\frac{e}{N_a}}$.

This section demonstrates that this kind of atom-light interaction creates an atomic spin squeezed state and consequently boosts the interferometer's performance. In the following section, we model the system more rigorously, using the freely propagating light field and including the effects of atomic spontaneous emission.
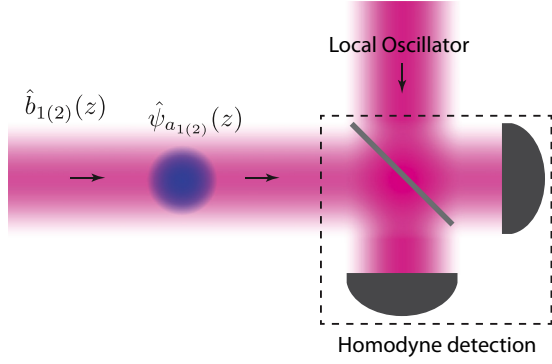
FIG. 3. Schematic of the free-space QND scheme. After interacting with the atomic ensemble, the freely propagating optical field is measured via homodyne detection.

IV. DETAILED MODEL DESCRIBING ATOM-LIGHT INTERACTION

We now consider a more detailed model that more accurately captures the relevant physics. In particular, in order to model propagating laser beams, we require a multimode model for the optical fields (see Fig. 3). We also include spontaneous emission from the excited atomic states, which will limit the amount of QND squeezing in practice.

A. Equations of motion describing atom-light interaction

We assume an ensemble of Bose-condensed atoms with two electronic states $|1\rangle$ and $|2\rangle$, coupled to excited states $|3\rangle$ and $|4\rangle$ respectively (Fig. 4). The coupling is achieved by far-detuned lasers, which are described by annihilation operators $\hat{b}_1(z, t)$ and $\hat{b}_2(z, t)$, satisfying the commutation relations $[\hat{b}_i(z, t), \hat{b}_j^\dagger(z', t)] = \delta_{ij}\delta(z - z')$ for $i, j = 1, 2$. We assume both optical fields have narrow linewidths compared to the natural linewidths of the atomic transitions, with central frequencies given by $\omega_{L_1} = \omega_{13} - \Delta_1$ and $\omega_{L_2} = \omega_{24} - \Delta_2$, where Δ_1 and Δ_2 are the detunings from the $|1\rangle \rightarrow |3\rangle$ and $|2\rangle \rightarrow |4\rangle$ transitions, respectively. The Hamiltonian for the total system after making the rotational-wave approximation
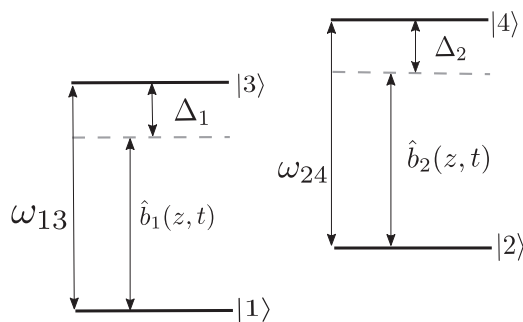

FIG. 4. Atomic energy diagram of the two two-level systems. Each atom is placed in a superposition of electronic states $|1\rangle$ and $|2\rangle$, with excited states $|3\rangle$ and $|4\rangle$. Two independent lasers (annihilation operators $\hat{b}_1$ and $\hat{b}_2$) are detuned from the $|1\rangle \rightarrow |3\rangle$ and $|2\rangle \rightarrow |4\rangle$ transitions by detuning Δ_1 and Δ_2, respectively.

(RWA) is

$$
\begin{aligned}
\hat{H}_{\text{tot}} = \hbar \int_{-\infty}^{\infty} dz(\omega_{13}\hat{\psi}_3^\dagger(z, t)\hat{\psi}_3(z, t) + \omega_{24}\hat{\psi}_4^\dagger(z, t)\hat{\psi}_4(z, t)) \\
- i\hbar c \int_{-\infty}^{\infty} \hat{b}_1^\dagger(z, t)\partial_z\hat{b}_1(z, t)dz \\
- i\hbar c \int_{-\infty}^{\infty} \hat{b}_2^\dagger(z, t)\partial_z\hat{b}_2(z, t)dz \\
+ \hbar g_{13} \int_{-\infty}^{\infty} (\hat{\psi}_1^\dagger(z, t)\hat{\psi}_3(z, t)\hat{b}_1^\dagger(z, t) + \text{H.c.})dz \\
+ \hbar g_{24} \int_{-\infty}^{\infty} (\hat{\psi}_2^\dagger(z, t)\hat{\psi}_4(z, t)\hat{b}_2^\dagger(z, t) + \text{H.c.})dz,
\end{aligned}
\tag{21}
$$

where $\hat{\psi}_i(z, t)$ is the field operator which annihilates an atom from atomic state $|i\rangle$ at position z, and $g_{13} = \frac{d_{13}}{\hbar}\left(\frac{\hbar\omega_{L_1}}{2\epsilon_0 A}\right)^{1/2}$ and $g_{24} = \frac{d_{24}}{\hbar}\left(\frac{\hbar\omega_{L_2}}{2\epsilon_0 A}\right)^{1/2}$ are the atom-light coupling constant, where $d_{13} = -e\langle 3|\hat{\mathbf{r}}|1\rangle$ and $d_{24} = -e\langle 4|\hat{\mathbf{r}}|2\rangle$ are the dipole moment matrix elements for the atomic transitions $|1\rangle \rightarrow |3\rangle$ and $|2\rangle \rightarrow |4\rangle$ respectively, A is the transverse quantization area of the light beam, and c is the speed of light.

For simplicity, in the following we will present the Heisenberg equations of motion just for one two-level system $\{|1\rangle \rightarrow |3\rangle, \hat{b}_1(z, t)\}$, since the two systems are decoupled in the sense that the Heisenberg equations of motion for $|1\rangle \rightarrow |3\rangle$ and $|2\rangle \rightarrow |4\rangle$ are independent. The corresponding equations hold for the second two-level system $\{|2\rangle \rightarrow |4\rangle, \hat{b}_2(z, t)\}$ as well.

We incorporate spontaneous emission as a Langevin term in our Heisenberg equation of motion by coupling the atoms being in their excited state to a reservoir of vacuum electromagnetic modes, which is then traced over, described by the Hamiltonian $\hat{H}_{\text{bath}} = \hbar \int_{-\infty}^{\infty} dz \int_{-\infty}^{\infty} d\omega\, \omega\, \hat{d}^\dagger(\omega, z)\hat{d}(\omega, z)$, where $\hat{d}(\omega, z)$ is the continuous in space and frequency annihilation operator of the bath satisfying $[\hat{d}(\omega, z), \hat{d}^\dagger(\omega', z')] = \delta(\omega - \omega')\delta(z - z')$. Hence, the equation of motion for $\hat{\psi}_3(z, t)$ in the presence of this Langevin term [72] is

$$
\begin{aligned}
\partial_t\hat{\psi}_3(z, t) = -\frac{i}{\hbar}[\hat{\psi}_3(z, t), \hat{H}_{\text{tot}}] \\
- \left[\frac{\gamma_3}{2}\hat{\psi}_3(z, t) + \sqrt{\gamma_3}\hat{d}_{1_{\text{in}}}(z, t)\right],
\end{aligned}
\tag{22}
$$

where γ_3 is the spontaneous emission rate from the excited state and $\hat{d}_{1_{\text{in}}}(z, t) = \frac{1}{\sqrt{2\pi}}\int_{-\infty}^{\infty} d\omega\, e^{-i\omega(t-t_0)}\hat{d}_0(\omega, z)$ is the standard Langevin noise term depending on the value of the bath operator at the initial time point t_0, $\hat{d}(\omega, z, t = t_0) = \hat{d}_0(\omega, z)$. After moving to a rotating reference frame, with respect to the central frequency of the light field, ω_{L_1}, we adiabatically eliminate the excited-state field operator $\hat{\psi}_3$ [73]. Thus, the Heisenberg equations of motion for $\hat{\psi}_1(z, t)$ and $\hat{b}_1(z, t)$ are

$$
\begin{aligned}
\partial_t\hat{\psi}_1(z, t) = ig_{13}^2 \frac{\Delta_1 + i\frac{\gamma_3}{2}}{\Delta_1^2 + \frac{\gamma_3^2}{4}}\hat{b}_1^\dagger(z, t)\hat{b}_1(z, t)\hat{\psi}_1(z, t) \\
+ g_{13}\frac{\sqrt{\gamma_3}}{\Delta_1 - i\frac{\gamma_3}{2}}\hat{b}_1^\dagger(z, t)\hat{d}_{1_{\text{in}}}(z, t),
\end{aligned}
\tag{23a}
$$

$$\left(\frac{1}{c}\partial_t + \partial_z\right)\hat{b}_1(z,t) = i\frac{g_{13}^2}{c}\frac{\Delta_1 + i\frac{\gamma_3}{2}}{\Delta_1^2 + \frac{\gamma_3^2}{4}}\hat{\psi}_1^\dagger(z,t)\hat{\psi}_1(z,t)\hat{b}_1(z,t)$$

$$+\frac{g_{13}}{c}\frac{\sqrt{\gamma_3}}{\Delta_1 - i\frac{\gamma_3}{2}}\hat{\psi}_1^\dagger(z,t)\hat{d}_{1_{\text{in}}}(z,t),$$

(23b)

where Δ_1 is the detuning of the transition from the ground to the excited state. We solve the equation for the light field by making the substitution $z \to z + ct$. As the timescale for the atomic dynamics is much slower than the timescale for the light to cross the atomic sample, we make the approximation that the light moves between two arbitrary points z_B to z_C instantaneously, i.e., $\hat{b}^\dagger(z_B,t)\hat{b}(z_B,t) = \hat{b}^\dagger(z_C,t)\hat{b}(z_C,t)$, as long as there is no atom-light interaction in $[z_B, z_C]$. In addition, as our system is a Bose-Einstein condensate, we assume that all the atoms are in the ground motional state of the trap, which allows us to make the single-mode approximation $\hat{\psi}_1(z,t) = u_0(z)\hat{a}_1(t)$. Assuming $\int_{z_L}^{z_R}|u_0(z)|^2 dz \approx 1$ for points z_L and z_R sufficiently far to the left and right of the atomic sample, respectively, we can write

$$\hat{b}_1(z_R,t) = \hat{b}_{01}(t)e^{i\frac{g_{13}^2}{c}(\Omega+i\Gamma)\hat{a}_1^\dagger(t)\hat{a}_1(t)}$$

$$+\frac{g_{13}}{c}\frac{\sqrt{\gamma_3}}{\Delta_1 - i\gamma_3/2}\hat{a}_1^\dagger(t)\hat{q}_{1_{\text{in}}}(t),$$

(24)

where we have considered the same motional function for the Langevin noise $\hat{d}_{1_{\text{in}}}(z,t) = u_0(z)\hat{q}_{1_{\text{in}}}(t)$. We have also defined $\hat{b}_{01}(t) = \hat{b}_1(z_L,t)$ and $\Omega \equiv \frac{\Delta_1}{\Delta_1^2 + \gamma_3^2/4}$, $\Gamma_3 \equiv \frac{\gamma_3/2}{\Delta_1^2 + \gamma_3^2/4}$ for notation simplicity. In order to find a simpler form for the atomic equation, Eq. (23a), we make the approximation that $\hat{b}_1^\dagger(z,t)\hat{b}_1(z,t) \approx \hat{b}_1^\dagger(z_L,t)\hat{b}_1(z_L,t)$; i.e., the number of photons in the mode does not change to a good approximation. Hence, after making the single-mode approximation again, we obtain

$$\partial_t\hat{a}_1(t) = ig_{13}^2(\Omega + i\Gamma)\hat{b}_{01}^\dagger(t)\hat{b}_{01}(t)\hat{a}_1(t)$$

$$+ g_{13}\frac{\sqrt{\gamma_3}}{\Delta_1 - i\frac{\gamma_3}{2}}\hat{b}_{01}^\dagger(t)\hat{q}_{1_{\text{in}}}(t).$$

(25)

B. Measurement of the optical observables

As in Sec. III, we notice that Eq. (24) indicates correlations between the atomic number and the phase of the light. We can define the phase quadrature for our multimode light field by selecting one specific mode. Specifically, we define $\hat{Y}_{\lfloor_1} = i(\hat{\lfloor}_1 - \hat{\lfloor}_1^\dagger)$ where

$$\hat{\lfloor}_1 = \int_0^\tau u_{\text{LO}}^*(t)\hat{b}_1(z_D,t)dt,$$

(26)

where z_D is the position of the photodetector. Also, $u_{\text{LO}}(t)$ corresponds to the temporal mode shape of the local oscillator used in the homodyne detection [74], satisfying

$$\int_0^\tau |u_{\text{LO}}(t)|^2 dt = c,$$

(27)

which ensures $[\hat{\lfloor}_1, \hat{\lfloor}_1^\dagger] = 1$ and consequently $[\hat{X}_{\lfloor_1}, \hat{Y}_{\lfloor_1}] = -2i$, where $\hat{X}_{\lfloor_1} = \hat{\lfloor}_1 + \hat{\lfloor}_1^\dagger$ is the corresponding amplitude

quadrature of $\hat{\lfloor}_1$. The most appropriate choice of local oscillator for this scheme is one with constant intensity with the frequency matched to the carrier frequency of our optical field, i.e.,

$$u_{\text{LO}}(t) = \sqrt{\frac{c}{\tau}}.$$

(28)

V. APPROXIMATE ANALYTIC SOLUTIONS

We can obtain an analytical estimate of the quantum-enhancement parameter, ξ_{s_2}, after making some approximations. Here we briefly present the basic intermediate steps we made in order to find out ξ_{s_2}, with and without spontaneous emission. A much more detailed presentation of these calculations can be found in the Appendixes A–C 4. For simplicity, we assume that the atom-light interaction strengths as well as the detunings are the same for the two atomic transitions, i.e., $g_{13} = g_{24} = g$ and $\Delta_1 = \Delta_2 = \Delta$ respectively. We also consider that initially the atoms and the light fields are in coherent states with the same amplitudes for the two atomic levels $\hat{a}_{1(2)}(0)|\alpha_{1(2)}\rangle = \sqrt{\frac{N_a}{2}}|\alpha_{1(2)}\rangle$ and for the light $\hat{b}_{01}(t)|\beta_1\rangle = \beta_0|\beta_1\rangle$, $\hat{b}_{02}(t)|\beta_2\rangle = \beta_0|\beta_2\rangle$, where we also assume that $\beta_0 = \beta_0^*$.

A. No spontaneous emission

Ignoring the effect of spontaneous emission (i.e., $\gamma_3 = 0$) vastly simplifies the problem and allows easy comparison with the simple single-mode model of Sec. III. In this case, the calculation of the atomic expectation values we are interested in is quite straightforward:

$$\langle\hat{N}_{a_1}(t)\rangle = \frac{N_a}{2}, \quad \langle\hat{N}_{a_1}^2(t)\rangle = \frac{N_a}{2}\left(1 + \frac{N_a}{2}\right).$$

(29)

We can also find the phase quadrature operator by making the small-angle approximation $\frac{g^2}{c\Delta}\hat{a}_1^\dagger(t)\hat{a}_1(t) \ll 1$:

$$\hat{Y}_1(\tau) \approx \hat{Y}_{1_{\text{in}}}(\tau) - \frac{g^2}{\sqrt{c\tau}\Delta}\hat{a}_1^\dagger(\tau)\hat{a}_1(\tau)\int_0^\tau[\hat{b}_{01}(t) + \hat{b}_{01}^\dagger(t)]dt,$$

(30)

where $\hat{Y}_{1_{\text{in}}}(\tau) = i\frac{\sqrt{c}}{\sqrt{\tau}}\int_0^\tau[\hat{b}_{01}(t) - \hat{b}_{01}^\dagger(t)]dt$.

Here we clearly notice that $\hat{Y}_1 \propto \hat{N}_{a_1}$. That supports our choice for the light signal to be $\hat{J}_z^{\text{inf}} \propto \hat{S}_b = \hat{Y}_2 - \hat{Y}_1$. Now, using Eqs. (29) and (30), we can calculate

$$\text{Var}(\hat{S}_b) \approx 2\text{Var}(\hat{Y}_1(\tau)) \approx 2 + 4\chi_{\text{ns}}^2 N_a N_{\text{ph}},$$

(31)

$$\text{Cov}(\hat{J}_z(\tau), \hat{S}_b(\tau)) = \text{Cov}(\hat{S}_b(\tau), \hat{J}_z(\tau)) \approx \chi_{\text{ns}} N_a\sqrt{N_{\text{ph}}},$$

(32)

$$\text{Var}(\hat{S}_2(\tau)) \approx \frac{N_a}{4}\left(1 - \frac{\chi_{\text{ns}}^2 N_{\text{ph}} N_a}{\chi_{\text{ns}}^2 N_{\text{ph}} N_a + 1/2}\right),$$

(33)

where here $N_{\text{ph}} = \beta_0^2\tau$. Also, we have defined $\chi_{\text{ns}} \equiv \frac{g^2}{c\Delta}$, where the subscript denotes no spontaneous emission. We finally find the quantum-enhancement parameter,

$$\xi_{s_2}^{\text{ns}}(\tau) \approx e^{\chi_{\text{ns}}^2 N_{\text{ph}}}\left(1 - \frac{\chi_{\text{ns}}^2 N_{\text{ph}} N_a}{\chi_{\text{ns}}^2 N_{\text{ph}} N_a + 1/2}\right)^{1/2},$$

(34)
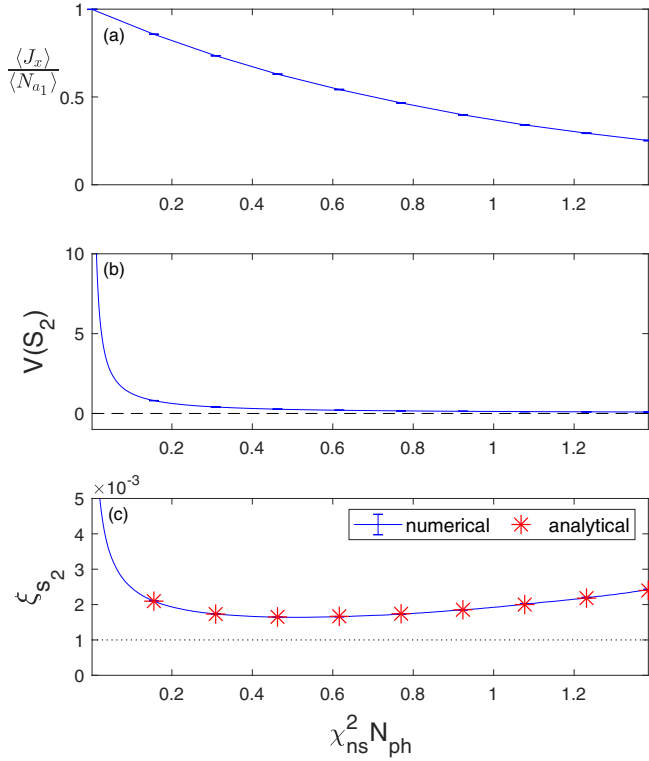
FIG. 5. (a) $\langle J_x \rangle / \langle N_{a_1} \rangle$, (b) Var$(S_2)$, and (c) ξ_{s_2} with respect to the collective parameter $\nu = \chi_{\text{ns}}^2 N_{\text{ph}}$. (a) The decay is due to oversqueezing the state, since we do not consider spontaneous emission here. This causes the squeezing parameter to reach a minimum value (c). The dashed line in panel (b) points to zero, just to assure the Var(S_2) is always positive. In panel (c), the dotted line represents the Heisenberg limit. The parameter values are $A = 10^{-10}$ m^2, $\Delta = 10^2$ GHz, $N_a = 10^6$. The error bars are barely distinguishable from all lines.

where we used that $\langle \hat{J}_x(t) \rangle \approx \frac{N_a}{2} e^{-\chi_{\text{ns}}^2 N_{\text{ph}}}$ for $\chi_{\text{ns}}^2 N_{\text{ph}} \ll 1$. By inspection of Eq. (34), we see that the parameters that affect the sensitivity of our signal are the total number of photons N_{ph}, the quantization area of the light field A (through g), the detuning Δ, and the total number of atoms N_a. We also notice that we can always increase the sensitivity of our signal by just increasing $\chi_{\text{ns}}^2 N_{\text{ph}} N_a$ up to a point that the increase of $e^{\chi_{\text{ns}}^2 N_{\text{ph}}}$ becomes dominant. This is essentially the point that $\langle J_x \rangle$ [denominator of Eq. (14)] has decreased so much that the sensitivity starts decaying. Following that strategy, we can always achieve better sensitivity than the standard quantum limit (SQL), as seen in Fig. 5. Here, we find the minimum of $\xi_{s_2}^{\text{ns}}$ by taking the derivative with respect to the collective parameter $\nu = \chi_{\text{ns}}^2 N_{\text{ph}}$:

$$(\xi_{s_2}^{\text{ns}})_{\text{min}} = \sqrt{\frac{e}{N_a}}. \quad (35)$$

We see that the minimum depends on the inverse of the number of atoms, while the optimum number of photons for which we take that minimum is

$$N_{\text{ph}}^{\text{opt}} = \frac{1}{2\chi_{\text{ns}}^2}. \quad (36)$$

B. Spontaneous emission

With the inclusion of spontaneous emission ($\gamma_3 > 0$), the calculation of the atomic expectation values is much more complicated. We begin by ignoring the effect that quantum fluctuation in the optical field has on the spontaneous emission. That is,

$$e^{-g^2 \Gamma \int_0^t \hat{b}^\dagger(z,t') \hat{b}(z,t') dt'} \approx e^{-g^2 \Gamma \beta_0^2 t} \quad (37)$$

such that

$$\langle \hat{N}_{a_1}(t) \rangle \approx \frac{N_a}{2} \epsilon(t), \quad (38)$$

where $\epsilon(t) \equiv e^{-2g^2 \Gamma \beta_0^2 t}$ indicates how quickly we lose atoms from our system. Following the same strategy as before, we find

$$\text{Var}(\hat{S}_b(\tau)) \approx 2 + 4\chi_1^2 N_{\text{ph}} N_a \overline{\epsilon(\tau)}, \quad (39)$$

$$\text{Cov}(\hat{J}_z(\tau), \hat{S}_b(\tau)) = \text{Cov}(\hat{S}_b(\tau), \hat{J}_z(\tau))$$
$$\approx \chi_1 \sqrt{N_{\text{ph}}} N_a \epsilon(\tau), \quad (40)$$

and

$$\text{Var}(\hat{S}_2(\tau)) \approx \frac{N_a}{4} \epsilon(\tau) \left(1 - \frac{\chi_1^2 N_{\text{ph}} N_a \epsilon(\tau)}{\chi_1^2 N_{\text{ph}} N_a \overline{\epsilon(\tau)} + 1/2} \right), \quad (41)$$

where we have defined $\chi_1 \equiv \frac{g^2 \Omega}{c}$ and $\overline{\epsilon(\tau)} = \frac{1}{\tau} \int_0^\tau \epsilon(t) dt$, which is the time average of the decay. Note that $\chi_1 = \chi_{\text{ns}}$ in the no spontaneous emission case ($\gamma_3 = 0$). By comparing Eq. (33) with (41), we realize that, other than the apparent effect of particle loss that the atomic spontaneous emission has on the dynamics of the system, there is an additional effect on the variance of the signal, caused by the emergence of the time-averaged decay rate in the denominator of Eq. (41), which cannot be reproduced from Eq. (33), by simply making the substitution $N_a \rightarrow N_a \epsilon(t)$. Using that $\langle \hat{J}_x(t) \rangle \approx \frac{N_a}{2} e^{-(\chi_1^2 + 2\chi_2) N_{\text{ph}}}$ for $(\chi_1^2 + 2\chi_2) N_{\text{ph}} \ll 1$, the spin-squeezing parameter is

$$\xi_{s_2} \approx e^{(\chi_1^2 + \chi_2) N_{\text{ph}}} \left(1 - \frac{\chi_1^2 N_{\text{ph}} N_a \epsilon(\tau)}{\chi_1^2 N_{\text{ph}} N_a \overline{\epsilon(\tau)} + 1/2} \right)^{1/2}, \quad (42)$$

where we have defined $\chi_2 \equiv \frac{g^2 \Gamma}{c}$ and now the decay factor can be expressed as $\epsilon(\tau) = e^{-2\chi_2 N_{\text{ph}}}$. We also find for the time average of the decay factor that $\overline{\epsilon(\tau)} = \frac{1 - \epsilon(\tau)}{2\chi_2 N_{\text{ph}}}$.

By inspecting Eq. (42), it is clear that the case with spontaneous emission is more complicated. We notice again that we can increase the sensitivity by increasing the term $\chi_1^2 N_{\text{ph}} N_a \propto \frac{N_{\text{ph}} N_a}{A^2 \Delta^2}$ (for $\Delta \gg \gamma_3$), but now we are restricted by the atomic loss rate $\epsilon = \exp(-2\chi_2 N_{\text{ph}}) \propto \exp(\frac{N_{\text{ph}}}{A\Delta^2})$ (for $\Delta \gg \gamma_3$). Hence, we have to find the appropriate parameter regime that balances between spin squeezing and atomic loss.

We present simulations of our analytical results for ξ_{s_2} [Figs. 6(c)–8(c)], for three different quantization area values, $A = (10^{-3}$ m$)^2$, $A = (10^{-4}$ m$)^2$, and $A = (10^{-5}$ m$)^2$. For each different area value, we essentially change the number of photons and detuning appropriately in order to obtain best sensitivities. For $A = (10^{-3}$ m$)^2$, we notice that we never obtain enhanced sensitivity (compared to SQL) since the loss

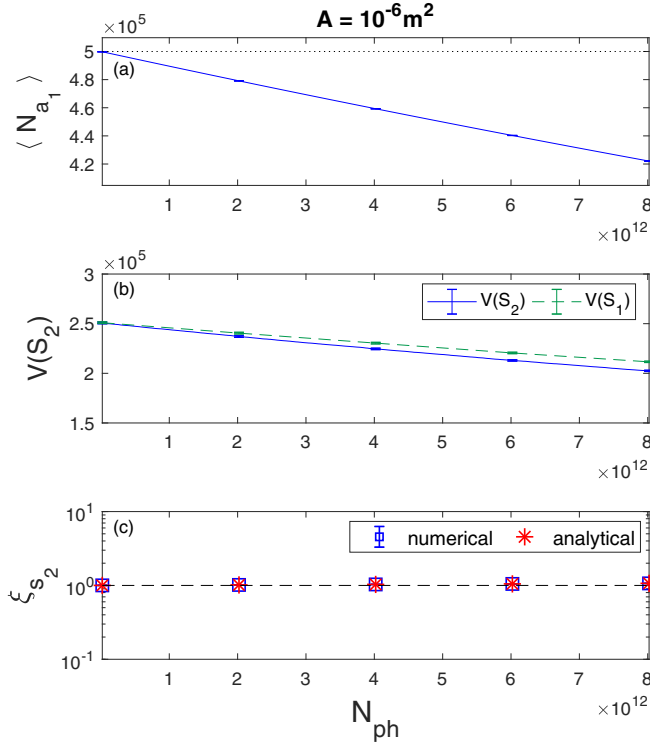FIG. 6. (a) $\langle N_{a_1} \rangle$, (b) Var(S_1) (green dashed line) and Var(S_2) (blue solid line), and (c) ξ_{s_2} numerical (blue squares) and analytical (red asterisks) with respect to number of photons. In panel (a), the black dotted line shows the initial atomic population, while the black dashed line in panel (c) represents the SNL. The parameter values are $A = 10^{-6}\,\mathrm{m}^2$, $\Delta = 10^2\,\mathrm{GHz}$, $N_a = 10^6$.

FIG. 7. (a) $\langle N_{a_1} \rangle$, (b) Var(S_1) (green dashed line) and Var(S_2) (blue solid line), and (c) ξ_{s_2} numerical (blue solid line) and analytical (red dashed line) with respect to number of photons. In panel (a), the black dotted line shows the initial atomic population, while the black dotted line in panel (c) represents the SNL. The parameter values are $A = 10^{-8}\,\mathrm{m}^2$, $\Delta = 10^2\,\mathrm{GHz}$, and $N_a = 10^6$.

of atoms exceeds the resulting squeezing [Fig. 6(c)]. As we decrease A, the atom-light interaction strengthens, increasing the sensitivity of our signal (Figs. 7 and 8).

In order to find the minimum of ξ_{s_2}, we express Eq. (42) in terms of the dimensionless parameters $\mu \equiv \frac{\chi_1^2}{\chi_2} = \frac{g^2\Omega^2}{c\Gamma}$, $\lambda \equiv \chi_2 N_{\mathrm{ph}}$, and $\zeta \equiv N_a \mu$. Hence, we can now write ξ_{s_2} as

$$\xi_{s_2} = e^{\lambda(1+\mu)} \left(1 - \frac{\zeta \epsilon(\tau)}{\zeta - \zeta \epsilon(\tau) + 1} \right)^{1/2}, \qquad (43)$$

where the decay can now be expressed as $\epsilon(\tau) = e^{-2\lambda}$. We work in a parameter regime where $\mu \ll 1$, such that

$$\xi_{s_2} \approx e^{\lambda} \left(1 - \frac{2\zeta \lambda e^{-2\lambda}}{1 + \zeta - \zeta e^{-2\lambda}} \right)^{1/2}. \qquad (44)$$

In order to simplify things further, we consider the case where $\Delta \gg \gamma_e$. In that case, $\Omega \to \frac{1}{\Delta}$ and $\Gamma \to \frac{\gamma_3}{2\Delta^2}$, and thus $\mu \to \frac{2g^2}{c\gamma_3}$. That means that μ only depends on the atomic properties and the quantization area of the light A (through g) and consequently $\zeta \to \frac{2g^2}{c\gamma_3} N_a$. On the other hand, $\lambda \to \frac{g^2\gamma_3}{2c} \frac{N_{\mathrm{ph}}}{\Delta^2}$ for $\Delta \gg \gamma_3$. Hence, if we fix the value of ζ by choosing a specific value for the number of atoms N_a and the area A, we only need to optimize ξ_{s_2} with respect to λ, which is proportional to N_{ph}/Δ^2 in the regime $\Delta \gg \gamma_3$. In Fig. 9, we followed that procedure for several different values of ζ and found the minimum of ξ_{s_2} with respect to λ using Eq. (44). We notice that
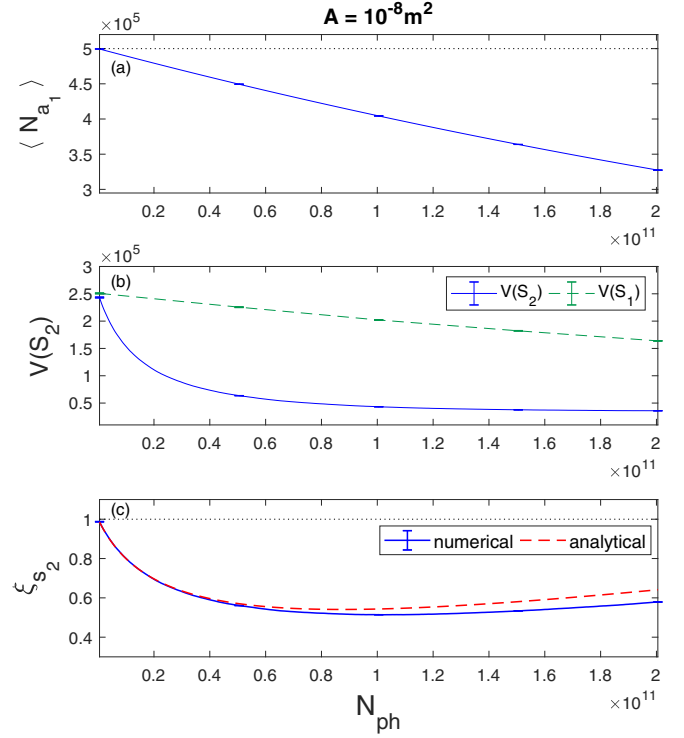
the sensitivity increases as we increase ζ, which means either increasing N_a or decreasing the area. Just to clarify here that by decreasing the area we also increase the atomic loss rate, which leads to loss of sensitivity. In that case, we should also change the other parameters (N_{ph}/Δ^2) in order to counteract that effect, resulting at the end in better sensitivities. On the other hand, the increase of N_a does not affect the loss rate of atoms and it solely improves the sensitivity.

We should mention here that there are similar analytical calculations available in the literature [75,76], but they are limited in the small atomic loss and Gaussian state regime, while our calculations go beyond these assumptions. In the following, we are going to present analytical and numerical results in the case of a phase squeezed light field, as well as numerical calculations including interactions amongst the atoms and the introduction of a cavity, which to our knowledge have not been examined before.

VI. NUMERICAL SOLUTIONS

We can solve for the dynamics of the system numerically by using the truncated Wigner (TW) method [77]. From the Heisenberg equations of motion, we can move to Fokker-Planck equations (FPEs) by using correspondences between quantum operators and Wigner variables. After truncating third and higher order terms, we can map the FPEs into stochastic differential equations (SDE) which can be solved numerically with respect to the Wigner variables. We make
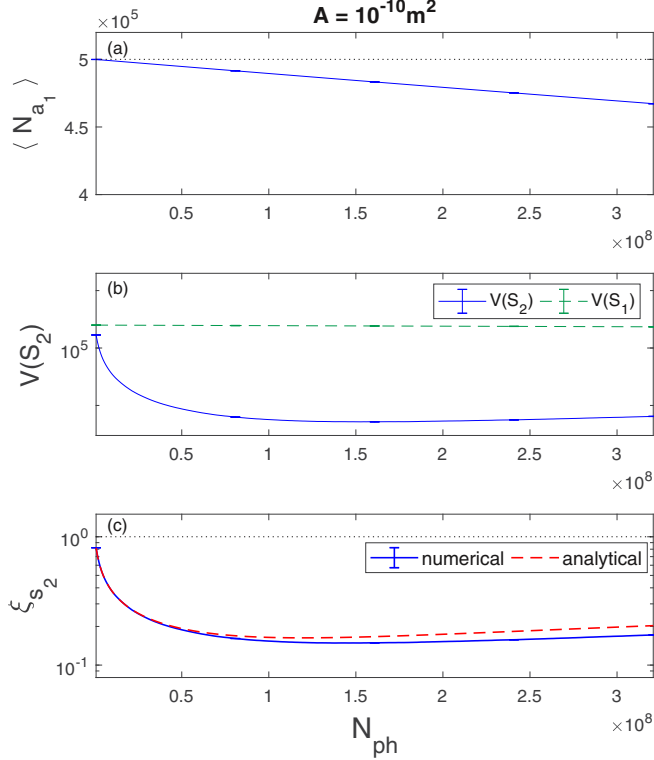
FIG. 8. (a) $\langle N_{a_1} \rangle$, (b) Var(S_1) (green dashed line) and Var(S_2) (blue solid line), and (c) ξ_{s_2} numerical (blue solid line) and analytical (red dashed line) with respect to number of photons. In panel (a), the black dotted line shows the initial atomic population, while the black dotted line in panel (c) represents the SNL. The parameter values are $A = 10^{-10}$ m^2, $\Delta = 10^2$ GHz, and $N_a = 10^6$.
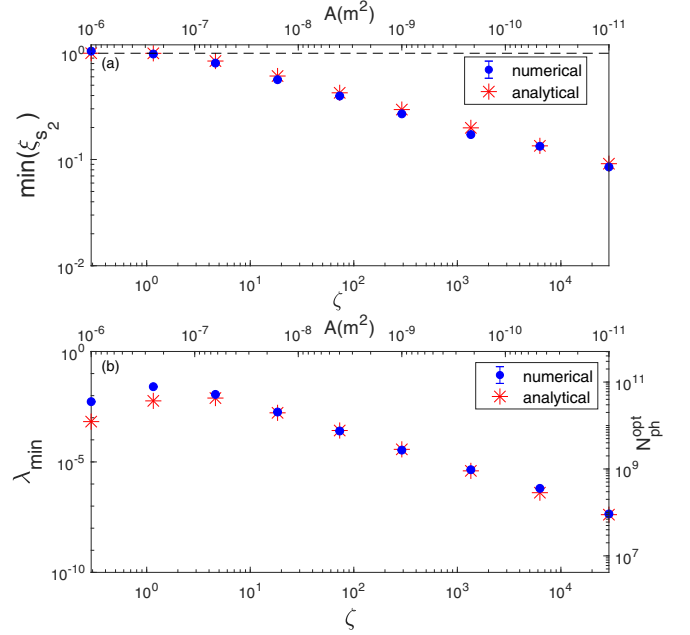

FIG. 9. (a) Minimum value of ξ_{s_2} with respect to ζ (bottom x axis) and A (top horizontal axis), (b) optimum λ (left vertical axis) and optimum number of photons $N_{\text{ph}}^{\text{opt}}$ (right y axis) with respect to ζ. In panel (a), the dashed line represents the SNL.

the following correspondences $\hat{a}_1(t) \to \alpha_1(t)$, $\hat{b}_1(z, t) \to \beta_1(z, t)$, and $\hat{q}_{1_{\text{in}}}(t) \to q_{\text{in}}(t)$. We also consider the initial conditions $\alpha_1(0) = \alpha_{10} + \eta_1$, $\beta_{01}(t) = \beta_0 + w_{b_1}(t)$, and $q_{\text{in}}(t) = w_{q_1}(t)$. η_1 is complex Gaussian noise satisfying $\overline{\eta_1} = 0$ and $\overline{\eta_1^* \eta_1} = \frac{1}{2}$; $w_x(t)$ is a complex Wiener noise satisfying $\overline{w_x(t)} = 0$, where $x = b_1, q_1$. Also, $\overline{w_{b_1}(t)w_{b_1}(t')} = \frac{1}{2c}\delta(t - t')$ and $\overline{w_{q_1}(t)w_{q_1}(t')} = \frac{1}{2}\delta(t - t')$, where the bar represents averaging with respect to a large number of stochastic trajectories.

We consider the $D2$ transition line of ^{87}Rb $(5^2S_{1/2} \to 5^2P_{3/2})$ for both atomic transitions, where the transition frequency is $\omega_{13} = \omega_{24} = \omega_a = 2\pi c/\lambda$ and $\lambda = 780$ nm. The spontaneous emission rate of the exited state is $\gamma_3 = \gamma_4 = 38.11$ MHz [78].

More particularly, we numerically examine the SDEs coming from Eqs. (24) and (25) for the light and the atoms respectively. For the atomic ensemble of each two-level system, we consider a single-mode field, while for the two light fields we make multimode simulations. Our numerical calculations give us the ability to examine the true dynamics of the system; namely, we consider the atomic spontaneous emission taking place during the unitary dynamics, which generates the spin squeezing. Most importantly, our numerical method enable us to introduce the new features in our system, considering the particle interactions of the two BECs (Sec. VII), examine the cavity case (Sec. IX), and explore how

they affect the final sensitivity, by numerically examining the more complicated dynamics.

In Figs. 6–9, we present the numerical simulations corresponding to the analytical results analyzed in the previous section. We notice that our analytical and numerical results have almost perfect agreement, indicating that the approximations we made through the derivations do not have any significant effect in the final results.

VII. BEC INTERACTIONS

So far the formalism we have developed could be applied equivalently to both BECs and cold thermal atoms homogeneously coupled to the light field, since essentially the only assumption we have made is that we work under the simple-mode approximation for the atomic ensembles of the two two-level systems. In this section, we examine how interactions among the particles of two BECs could affect the dynamics of the QND measurement scheme and how that could change the results we have already presented. We consider that these interactions are described by a Hamiltonian of the form

$$\hat{H}_{\text{BEC}}^{\text{int}} = \sum_{i,j=1,2} \frac{U_{ij}}{2} \int_{-\infty}^{\infty} \hat{\psi}_i^\dagger(\mathbf{r})\hat{\psi}_j^\dagger(\mathbf{r})\hat{\psi}_i(\mathbf{r})\hat{\psi}_j(\mathbf{r}) \, dz, \quad (45)$$

where $U_{ij} = \frac{4\pi\hbar^2}{m} a_{ij}$ is the nonlinear interaction potential and a_{ij} is the s-wave scattering length between $|i\rangle$ and $|j\rangle$, with $i, j = 1, 2$. In the previous sections, we worked under the assumption that the light field propagates only toward the z axis and hence we could analyze the dynamics of the atom-light interactions in the one-dimensional (1-D) case. However, here we focus on the interactions among the atoms of the two BECs, and we develop a three-dimensional (3-D) analysis,

since we consider that each atomic ensemble forms a sphere of radius r_{BEC}. We make the single-mode approximation for both BECs, as we did previously:

$$\hat{\psi}_1(z,t) = u_{01}(\boldsymbol{r})\hat{a}_1(t), \qquad \hat{\psi}_2(z,t) = u_{02}(\boldsymbol{r})\hat{a}_2(t). \quad (46)$$

Substituting that back in Eq. (45), we obtain

$$\hat{H}_{\mathrm{BEC}}^{\mathrm{int}} = \hbar\chi_{11}\hat{a}_1^\dagger(t)\hat{a}_1^\dagger(t)\hat{a}_1(t)\hat{a}_1(t) + \hbar\chi_{22}\hat{a}_2^\dagger(t)\hat{a}_2^\dagger(t)\hat{a}_2(t)\hat{a}_2(t)$$
$$+ 2\hbar\chi_{12}\hat{a}_1^\dagger(t)\hat{a}_1(t)\hat{a}_2^\dagger(t)\hat{a}_2(t), \quad (47)$$

where we defined

$$\chi_{ij} = \frac{U_{ij}}{2\hbar}\int_{-\infty}^{\infty}|u_{0i}(\boldsymbol{r})|^2|u_{0j}(\boldsymbol{r})|^2\,d^3\boldsymbol{r}. \quad (48)$$

Alternatively, we can use the number density of atoms in order to write

$$\int_{-\infty}^{\infty}|u_{0i}(\boldsymbol{r})|^2|u_{0j}(\boldsymbol{r})|^2\,d^3\boldsymbol{r} = \frac{1}{N_iN_j}\int_{-\infty}^{\infty}n_i(\boldsymbol{r})n_j(\boldsymbol{r})\,d^3\boldsymbol{r}. \quad (49)$$

Assuming constant number density, we finally find

$$\chi_{11} = \frac{2\pi\hbar}{mV}a_{11}, \qquad \chi_{22} = \frac{2\pi\hbar}{mV}a_{22}, \quad (50)$$

which represents the strength of the intraparticle interactions in each BEC. If we consider that there are no interparticle interactions, namely the two BECs are separate, then $\chi_{12} = 0$, while if we assume that they are perfectly overlapping, then $\chi_{12} = \frac{2\pi\hbar}{mV}a_{12}$. The Hamiltonian in Eq. (47) would add the following terms in the atomic equations of motion for the two two-level systems,

$$\partial_t\hat{a}_1(t) = -2i(\chi_{11}\hat{a}_1^\dagger(t)\hat{a}_1(t) + \chi_{12}\hat{a}_2^\dagger(t)\hat{a}_2(t))\hat{a}_1(t), \quad (51)$$

$$\partial_t\hat{a}_2(t) = -2i(\chi_{22}\hat{a}_2^\dagger(t)\hat{a}_2(t) + \chi_{12}\hat{a}_1^\dagger(t)\hat{a}_1(t))\hat{a}_2(t). \quad (52)$$

Hence, now we can numerically examine the full dynamics of the system, with the BEC interactions incorporated, using again the TW method. We can essentially do that by transforming the above operator equations of motion into a FPE and map the result to a SDE, as we did earlier. We add the resulted terms in the SDEs of the previous sections, in order to examine the full dynamics. In our simulations, we considered the same scattering lengths as in Refs. [52,79], namely $a_{11} = 100.4\,a_0$, $a_{22} = 95.00\,a_0$, and $a_{12} = 97.66\,a_0$, where a_0 is the Bohr radius. We also assumed that the area of the atomic ensemble should be smaller or equal than the transverse area of the light field. In our numerical calculations, we used $A_{\mathrm{BEC}} = 10^{-11}$ m^2, corresponding to a radius $r_{\mathrm{BEC}} = 2\,\mu$m for the BEC.

In the previous sections, in the absence of BEC interactions, we noticed that for fixed values of the area (A), the detuning (Δ), and the number of atoms (N_a), we can find the minimum of the squeezing parameter by adjusting the number of photons. That means that the change of the total time of interaction was equivalent with the change of the light intensity. However, now that we consider interactions among the atoms, the time would play a more crucial role in the dynamics, since after some time the atom interactions would become significant, resulting in a decrease of the final sensitivity. This is shown in Fig. 10(a), where we notice that considering intraparticle interactions in two separate BECs
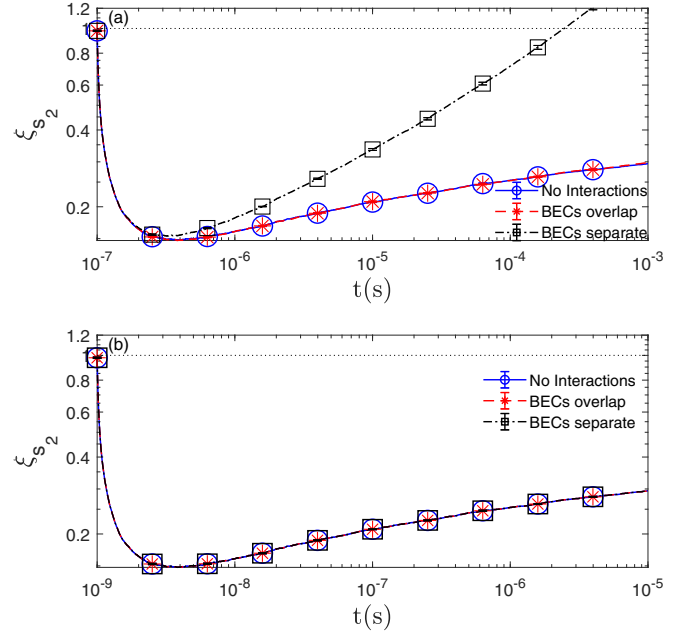

FIG. 10. ξ_{s_2} with respect to time considering three different cases, (i) no atom interactions (blue solid line with open circles), (ii) atom interactions where the two BECs perfectly overlap (red dashed line with asterisks) and (iii) atom interactions, where the two BECs are separate (black dash-dotted line with squares). In panel (a), we consider smaller light intensity and larger total interaction time compared to panel (b); i.e., in panel (a) we have $\beta_0^2 = 10^{12}$ photons/s and $\tau = 1$ms, while in panel (b) $\beta_0^2 = 10^{14}$ photons/s and $\tau = 0.01$ ms. The other parameter values are: $N_a = 10^6$, $\Delta = 10^{11}$, $A = 10^{-10}$ m^2, and $A_{\mathrm{BEC}} = 10^{-11}$m^2. The black dotted lines denote the SNL.

degrades the sensitivity, while the case of two overlapping BECs perfectly coincides with the no-interaction case, since the total interaction strength among the atoms is smaller compared to the two separate BECs case. As aforementioned, the number of photons interacting with the atomic ensemble is what really matters, since it determines the level of squeezing we obtain in the QND measurement scheme. Hence, we can easily find an appropriate regime, in order to avoid the deleterious effects of atom interactions to the final sensitivity, by increasing the light intensity and appropriately decreasing the total interaction time. In that way, we consider the same number of photons, offering the same level of spin squeezing, while everything happens more quickly, which means that there is not enough time for the atom interactions to damage the final sensitivity, as shown in Fig. 10(b).

VIII. SQUEEZED LIGHT

Up to this point, we have only considered classical light sources. That is, we have assumed that the incoming light is a coherent state, with $\mathrm{Var}(\hat{Y}_{1_{\mathrm{in}}}) = 1$. It is possible to increase the sensitivity of our final signal by considering a squeezed incoming light, where $\mathrm{Var}(\hat{Y}_{1_{\mathrm{in}}})_{\mathrm{sq}} = e^{-2r}$ and r is the squeezing factor [74]. In that case, our analytical calculation for the spontaneous emission case results in

$$\mathrm{Var}(\hat{S}_b)_{\mathrm{sq}} \approx 2\mathrm{Var}(\hat{Y}_1(\tau))_{\mathrm{sq}} \approx 2e^{-2r} + 4\chi_{\mathrm{ns}}^2N_aN_{\mathrm{ph}}, \quad (53)$$
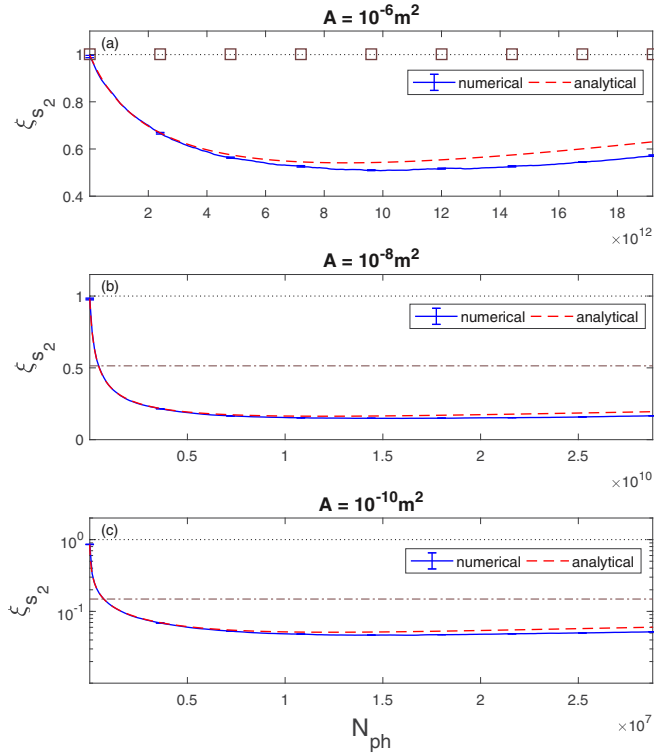
FIG. 11. We consider squeezed incoming light and we examine the numerical (blue solid line) and analytical (red dashed line) evolution of ξ_{s_2} with respect to the number of photons for all three area values. The brown squares in panel (a) and brown dash-dotted lines in panels (b) and (c) show the $\min(\xi_{s_2})$ of the corresponding cases in Figs. 6–8. The black dotted lines denote the SNL. The other parameter values are $r = \ln 10$, $\Delta = 10^2$ GHz, and $N_a = 10^6$.

while the covariances remain the same. Hence, the quantum enhancement parameter becomes

$$\xi_{s_2} \approx e^{(\chi_1^2 + \chi_2)N_{\mathrm{ph}}} \left(1 - \frac{\chi_1^2 N_{\mathrm{ph}} N_a \epsilon(\tau)}{\chi_1^2 N_{\mathrm{ph}} N_a \overline{\epsilon(\tau)} + e^{-2r}/2}\right)^{1/2}. \quad (54)$$

In Fig. 11, we notice that we obtain better sensitivity for all three area values compared to the coherent incident light (Figs. 6–8). In Fig. 12, we show the numerical and analytical $\min(\xi_{s_2})$ for the three different area values, with respect to the degree of optical squeezing in the incoming light, $\mathcal{S}$, defined by

$$\mathcal{S} = 10 \log \left(\frac{\sqrt{\mathrm{Var}(\tilde{Y}_{b_1})}}{\sqrt{\mathrm{Var}(Y_{b_1})}}\right) \mathrm{dB}, \quad (55)$$

where $\mathrm{Var}(Y_{b_1}) = 1$ is the variance for a coherent state, and $\mathrm{Var}(\tilde{Y}_{b_1}) = e^{-2r}$, where r is the squeezing factor. Using squeezed incoming light gives an exponential rate of decrease for ξ_s for all cases (for $A = 10^{-6}$ that holds for $\gtrsim 5$ dB). In addition, for a light field with improvement $\gtrsim 5$ dB, we see that we can surpass the SNL even for the $A = 10^{-6}$ m^2 case, while that was impossible when we used a coherent initial state for the light field [Fig. 6(c)]. Finally, we notice in Fig. 12 that our analytical approximative model (red stars) given by Eq. (54) agrees well with our numerical results (blue circles).
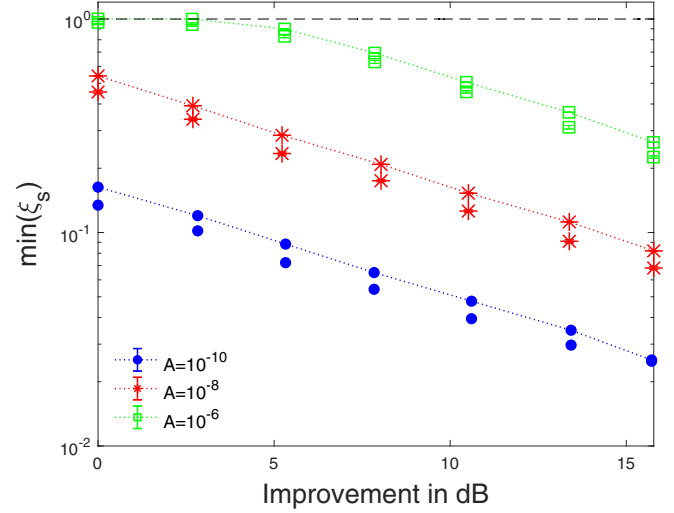

FIG. 12. Analytical (dotted lines with markers) and numerical (markers) calculation of the minimum value of ξ_{s_2} with respect to the improvement in dB of the incoming light field, for the three different area values. The dashed line represents the SNL. The other parameter values are $\Delta = 10^2$ GHz, $N_a = 10^6$.

IX. CAVITY DYNAMICS

We can further boost the sensitivity of our signal with the addition of an optical cavity, as it essentially increases the atom-light coupling (Fig. 13). We consider a dual-frequency cavity with resonant frequencies ω_{c_1} and ω_{c_2} detuned from the two atomic transitions $|1\rangle \rightarrow |3\rangle$ and $|2\rangle \rightarrow |4\rangle$ by detunings Δ_1 and Δ_2 respectively. In the Hamiltonian of our system, Eq. (21), we interchange the continuous light field annihilation operators $\hat{b}_1(z, t)$ and $\hat{b}_2(z, t)$ with the cavity mode annihilation operator $\hat{c}_1$ and $\hat{c}_2$, giving

$$\hat{H}_{\mathrm{tot}}^c = \hbar \omega_{c_1} \hat{c}_1^\dagger \hat{c}_1 + \hbar \omega_{c_2} \hat{c}_2^\dagger \hat{c}_2$$

$$+ \hbar \int_{-\infty}^{\infty} dz (\omega_{13} \hat{\psi}_3^\dagger(z, t) \hat{\psi}_3(z, t)$$

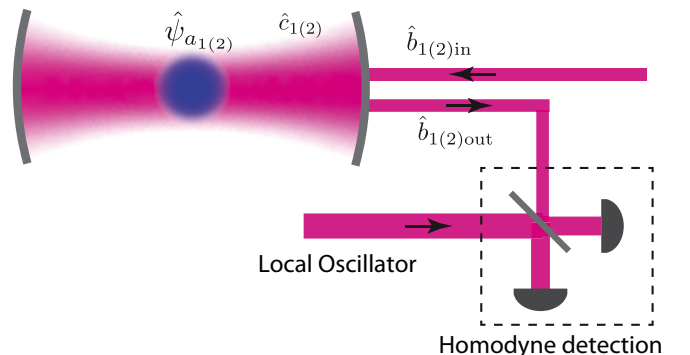$$+ \omega_{24} \hat{\psi}_4^\dagger(z, t) \hat{\psi}_4(z, t))$$

FIG. 13. QND interaction boosted by an optical cavity. After interacting with the atomic ensemble, the light exiting the cavity $\hat{b}_{1(2)\mathrm{out}}$ is measured via homodyne detection.

$$+ \hbar g_{c_1} \int_{-\infty}^{\infty} (\hat{\psi}_1^\dagger(z,t)\hat{\psi}_3(z,t)\hat{c}_1^\dagger(t) + \text{H.c.})dz$$

$$+ \hbar g_{c_2} \int_{-\infty}^{\infty} (\hat{\psi}_2^\dagger(z,t)\hat{\psi}_4(z,t)\hat{c}_2^\dagger(t) + \text{H.c.})dz. \quad (56)$$

The coupling strength constants are defined as $g_{c_1} = \frac{d_{13}}{\hbar}(\frac{\hbar\omega_{c_1}}{2\epsilon_0 V})^{1/2}$ and $g_{c_2} = \frac{d_{24}}{\hbar}(\frac{\hbar\omega_{c_2}}{2\epsilon_0 V})^{1/2}$, where $V = AL$ is the volume of the cavity, A is the light quantization transverse area, and L is the cavity length. Using the standard input output formalism [80], we obtain the equation of motion for $\hat{c}_1$,

$$\partial_t \hat{c}_1 = -\frac{i}{\hbar}[\hat{c}_1, \hat{H}_{\text{tot}}^c] - \frac{\kappa}{2}\hat{c}_1 + \sqrt{\kappa}\hat{b}_{1_{\text{in}}}(t), \quad (57)$$

where κ is the cavity photon decay rate, and $\hat{b}_{1_{\text{in}}}(t) = \sqrt{c}\hat{b}_1(z_L, t)$, where c is the speed of light and $\hat{b}_1(z_L, t)$ is the continuous in space annihilation operator of the incoming light field used in the previous sections, satisfying $[\hat{b}_{1_{\text{in}}}(t), \hat{b}_{1_{\text{in}}}(t')] = \delta(t - t')$. Another important quantity is the light field leaking out of the cavity:

$$\hat{b}_{1_{\text{out}}}(t) = \sqrt{\kappa}\hat{c}_1(t) - \hat{b}_{1_{\text{in}}}(t). \quad (58)$$

In this case, $\hat{b}_{1_{\text{in}}}(t)$ is an input light field that coherently drives the dynamics of the cavity, but now the mode of the cavity, $\hat{c}_1$, is the one that interacts with the atomic ensemble and is entangled with the atomic ground-state number operator. Again, we incorporate spontaneous emission following the same method as in Sec. IV; i.e., we use Eq. (22) in order to eliminate $\hat{\psi}_3(z, t)$ from the equations of motion for $\hat{\psi}_1(z, t)$ and $\hat{c}_1$. After making the single-mode approximation for $\hat{\psi}_1(z, t)$ and $\hat{d}_{1_{\text{in}}}(z, t)$ using again the same mode functions for both of them and moving to a rotating frame with respect to the cavity resonance frequency, we obtain

$$\partial_t \hat{a}_1(t) = ig^2(\Omega + i\Gamma)\tilde{c}_1^\dagger(t)\tilde{c}_1(t)\hat{a}_1(t)$$

$$+ g_c\frac{\sqrt{\gamma_3}}{\Delta_1 - i\gamma_3/2}\tilde{c}_1^\dagger(t)\tilde{q}_{1_{\text{in}}}(t), \quad (59a)$$

$$\partial_t \tilde{c}_1(t) = \left[ig^2(\Omega + i\Gamma)\hat{a}_1^\dagger\hat{a}_1 - \frac{\kappa}{2}\right]\tilde{c}_1(t)$$

$$+ g_c\frac{\sqrt{\gamma_3}}{\Delta_1 - i\gamma_3/2}\hat{a}_1^\dagger(t)\tilde{q}_{1_{\text{in}}}(t) + \sqrt{\kappa}\,\tilde{b}_{1_{\text{in}}}(t), \quad (59b)$$

where $\tilde{c}_1(t) = \hat{c}(t)e^{i\omega_{c_1}t}$, $\tilde{b}_{1_{\text{in}}}(t) = \hat{b}_{1_{\text{in}}}(t)e^{i\omega_{c_1}t}$, and $\tilde{q}_{1_{\text{in}}}(t) = \hat{q}_{1_{\text{in}}}(t)e^{i\omega_{c_1}t}$.

To investigate the dynamics, we use the TW method, again making the appropriate correspondences, in order to numerically examine the dynamics of our system. In Fig. 14, we plot the time evolution of the number of atoms and the number of cavity photons as well as the intensity of the input and output fields. We see that the cavity comes into its steady state after time $t \gg 1/\kappa$. As such, the rate of incoming photons should be larger than the rate of loss, i.e., $\langle \hat{b}_{1_{\text{in}}}^\dagger \hat{b}_{1_{\text{in}}}\rangle \gg \kappa$, to ensure $\langle \hat{N}_{c_1}\rangle = \langle \hat{c}_1^\dagger \hat{c}_1\rangle \gg 1$. In our numerical simulations, we have fixed the total interaction time $\tau = 10^{-4} \gg 1/\kappa = 10^{-6}$ and we change the number of cavity photons, which is the parameter affecting the dynamics of our system, by just changing the intensity of the incoming light field $\langle \hat{b}_{1_{\text{in}}}^\dagger \hat{b}_{1_{\text{in}}}\rangle$.

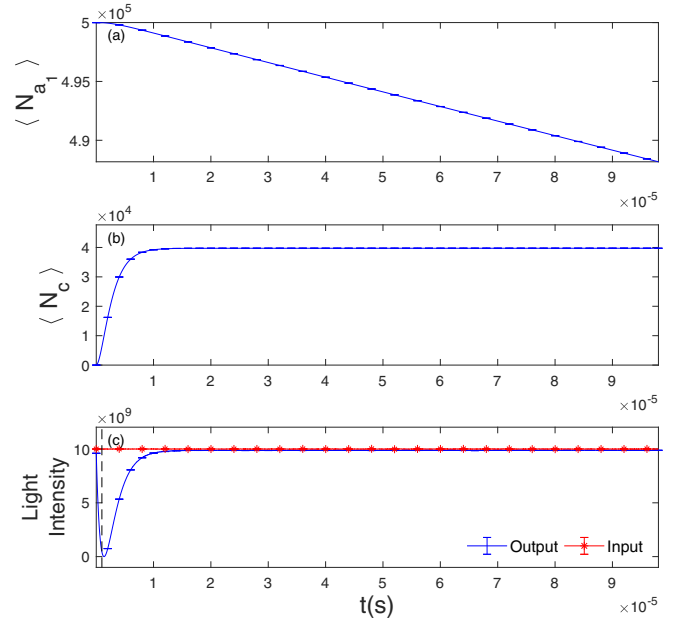We measure a combined signal of the same form as in the free space case, but now we measure an observable of the

FIG. 14. Cavity dynamics: time evolution of (a) mean number of atoms in state $|1\rangle$, $\langle N_{a_1}\rangle$, (b) mean number of cavity photons $\langle N_{c_1}\rangle$, (c) intensity of input light (red solid line with asterisks) and intensity of the leaking output light field from the cavity (blue solid line). The vertical black dashed line is drawn at the time point $1/\kappa$. We notice that we need $\tau \gg 1/\kappa$, in order to reach the cavity steady state. Other parameter values are $A = 10^{-8}$ m^2, $\Delta = 10^2$ GHz, $N_a = 10^6$, and $\kappa = 1$ MHz.

output field, $\hat{b}_{1_{\text{out}}}(t)$, since we do not have any direct access to the cavity mode. The output field contains information about atomic observables through Eq. (58). Like in Sec. (IV B), we use as our light observable the difference of the phase quadratures of a specific mode of the output fields.

We plot ξ_{s_2} for the same area values as for Figs. 6–8 with $\kappa = 10^6$ Hz. Here, we noticed that for $\Delta = 10^2$ GHz and area values smaller than $A = 10^{-8}$ m^2 we have to decrease the incoming light intensity at a level that we tend to a regime where $\langle \hat{N}_{c_1}\rangle \to 1$. We can avoid that by just appropriately increasing the detuning $\Delta = 10^4$ GHz, in order to obtain the same interaction strength. Assuming a cavity of length $L = 10$ cm, this corresponds to a finesse of $\approx 10^4$. Our choice of cavity parameters is similar to those reported in Ref. [81], and is motivated by a cavity that could be added to an existing atom interferometry setup and can be installed outside the vacuum system. We use a range of different intensities for the incoming light field to determine the best sensitivity. Comparing Figs. 6–8 with Fig. 15, it is apparent that we achieve better sensitivities by adding a cavity than just by using free space light fields. Although we do not have any analytical results for the case of the cavity, due to the complexity of that model, we examined numerically if the dynamics of the system has the same behavior as in the free space case. We concluded that we can find the optimum of the sensitivity using the same procedure as in Sec. VI. Namely, for particular values of A (or equivalently $V = AL$) and N_a, we can find the minimum of ξ_{s_2} with respect to the remaining parameters N_{c_1}/Δ_1^2. Here we have one parameter more, the photon decay rate from
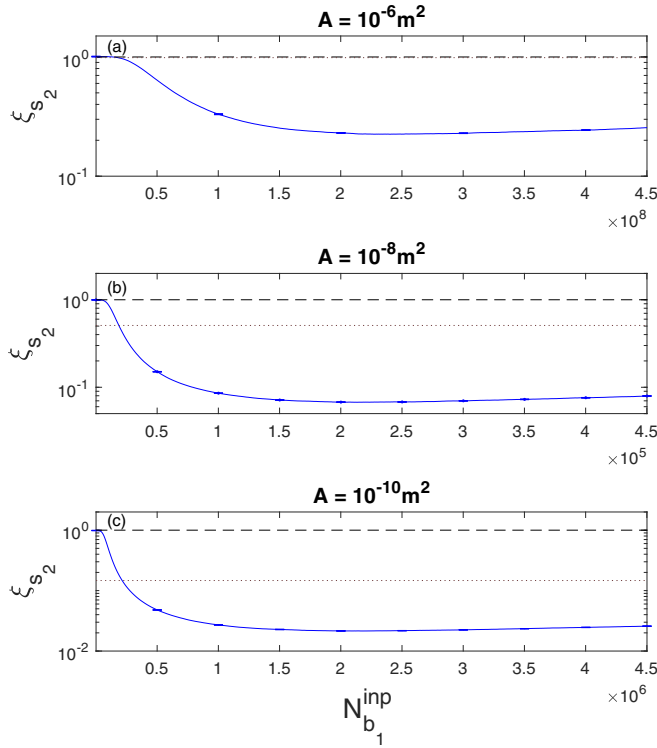
FIG. 15. Cavity: ξ_s with respect to $N_{b_1}^{\text{inp}}$ for different values of A. The brown dotted lines show the $\min(\xi_{s_2})$ of the corresponding cases in Figs. 6–8. The black dashed lines represent the SNL. The parameter values are $N_a = 10^6$, $\kappa = 1$ MHz, and $\Delta = 10^2$ GHz, except in panel (c), where we used $\Delta = 10^4$ GHz, for the reasons discussed in the main text.

the cavity, κ. We notice that we have better sensitivities for smaller values of κ and thus for larger cavity quality factors (see Fig. 16). However, in the cavity case, we are more constrained on the parameter values we could use, as they should satisfy $\langle \hat{b}_{1_{\text{in}}}^{\dagger} \hat{b}_{1_{\text{in}}} \rangle > \kappa$ and $\tau > 1/\kappa$ as we discussed earlier.

X. CONCLUSION

We have analyzed the creation of spin squeezing in an ensemble of Bose-condensed atoms via quantum nondemolition measurement, considering both freely propagating light and optical cavities. We found that the determining factor in the quality of spin squeezing produced was the cross-sectional area of the optical beam used to probe the spin of the atomic system, with small areas leading to higher atom-light coupling and a larger phase shift on the light for a given level of spontaneous emission. Of course, varying the intensity, detuning, or duration of the incoming light also affects the level of spin squeezing. However, for a given area, fixing two of these parameters while adjusting the remaining one would always lead to the same optimum. For the $D2$ transition in ^{87}Rb atoms, we found that for the case of freely propagating light, no squeezing was possible when the cross-sectional area of the atom-light interaction was larger than $\approx 10^{-6}$ m^2 because of the loss of atoms due to spontaneous emission, regardless of the intensity or detuning of the incoming light. For areas less than this, we found significant spin squeezing was possible,
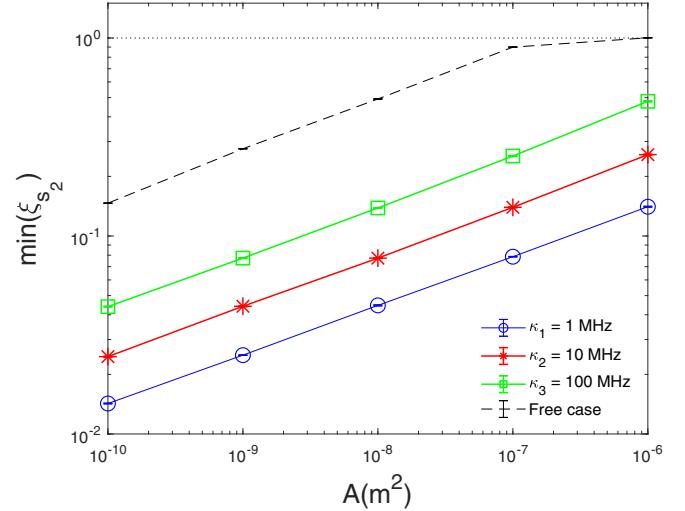

FIG. 16. Minimum value of ξ_{s_2} with respect to the area, for three different values of κ for the cavity case. We also plot the free space case (black dashed line). The black dotted line represents the SNL. The other parameter values are $N_a = 10^6$ and $\Delta = 10^2$ GHz, except for the area values $A = 10^{-9}$ m^2 and $A = 10^{-10}$ m^2 in all cavity lines where we used $\Delta = 10^4$ GHz, for the reasons we mentioned in the main text.

with an area of 10^{-11} m^2 leading to a spin-squeezing value of $\approx 3 \times 10^{-2}$, which corresponds to a potential improvement of atom interferometric sensitivity of ≈ 33, which is equivalent to increasing the number of atoms by a factor of 1000. The use of optical squeezing improved the level of quantum enhancement further and relaxed the restrictions on the area of the light. Finally, we considered the use of an optical cavity. For reasonably achievable cavity parameters, we found approximately an order of magnitude increase over what was achievable in the free space case.

ACKNOWLEDGMENTS

APPENDIX A: INTRODUCTION

We consider the combined signal

$$\hat{S}_2(\tau) = \hat{J}_z(\tau) - \hat{J}_z^{\text{inf}}(\tau), \tag{A1}$$

where

$$\hat{J}_z^{\text{inf}}(\tau) = G\hat{S}_b(\tau), \quad \hat{S}_b(\tau) = \hat{Y}_2(\tau) - \hat{Y}_1(\tau). \tag{A2}$$

For simplicity, in the following we will present the time dependence explicitly only in our final results or when it is considered necessary. The variance of $\hat{S}_2$ would be given by

$$\text{Var}(\hat{S}_2) = \text{Var}(\hat{J}_z) + G^2 \text{Var}(\hat{S}_b) - 2G\text{Cov}(\hat{J}_z, \hat{S}_b), \tag{A3}$$

since $\mathrm{Cov}(\hat{J}_z, \hat{S}_b) = \mathrm{Cov}(\hat{S}_b, \hat{J}_z)$. We minimize $\mathrm{Var}(\hat{S}_2)$ with respect to G:

$$G = \frac{\mathrm{Cov}(\hat{J}_z, \hat{S}_b)}{\mathrm{Var}(\hat{S}_b)}. \tag{A4}$$

Inserting that back in Eq. (A3), we get

$$\mathrm{Var}(\hat{S}_2) = \mathrm{Var}(\hat{J}_z) - \frac{\mathrm{Cov}^2(\hat{J}_z, \hat{S}_b)}{\mathrm{Var}(\hat{S}_b)}. \tag{A5}$$

So, in order to calculate $\mathrm{Var}(\hat{S}_2)$, we need the covariance between $\hat{J}_z$ and $\hat{S}_b$, $\mathrm{Cov}(\hat{J}_z, \hat{S}_b)$, and the variance of the phase quadrature of the light field $\mathrm{Var}(\hat{Y}_1)$, since $\mathrm{Var}(\hat{Y}_1) = \mathrm{Var}(\hat{Y}_2)$ and $\mathrm{Cov}(\hat{Y}_2, \hat{Y}_1) = 0$; thus, $\mathrm{Var}(\hat{S}_b) = 2\mathrm{Var}(\hat{Y}_1)$. At the end, we calculate the squeezing parameter, which in our case ($\theta = 0$) is given by

$$\xi_{s_2} = \sqrt{N_a} \frac{\sqrt{\mathrm{Var}(\hat{S}_2)}}{\langle \hat{J}_x \rangle}. \tag{A6}$$

APPENDIX B: NO SPONTANEOUS EMISSION

1. Atomic expectation values

The atomic equations with no spontaneous emission are given by

$$\hat{a}_1(t) = \hat{a}_1(0)e^{i\frac{g^2}{\Delta}\int_0^t \hat{b}_{01}^\dagger(t')\hat{b}_{01}(t')dt'}, \tag{B1}$$

$$\hat{a}_1^\dagger(t) = \hat{a}_1^\dagger(0)e^{-i\frac{g^2}{\Delta}\int_0^t \hat{b}_{01}^\dagger(t')\hat{b}_{01}(t')dt'}. \tag{B2}$$

Hence, the atomic population operator is independent of time:

$$\hat{N}_{a_1}(t) = \hat{a}_1^\dagger(t)\hat{a}_1(t) = \hat{a}_1^\dagger(0)\hat{a}_1(0). \tag{B3}$$

We consider that our total state initially is given by the product

$$|\Psi\rangle = |\alpha_1\rangle \otimes |\alpha_2\rangle \otimes |\beta_1\rangle \otimes |\beta_2\rangle \otimes |0\rangle, \tag{B4}$$

meaning that the atomic ensemble, as well as the two light fields, are in coherent states while the bath is described by the vacuum state, giving the following expectation values:

$$\hat{a}_1(0)|\alpha_1\rangle = \sqrt{\frac{N_a}{2}}|\alpha_1\rangle, \quad \hat{b}_{01}(t)|\beta_1\rangle = \beta_0|\beta_1\rangle,$$

$$\hat{q}_{1_{\mathrm{in}}}(t)|0\rangle = 0|0\rangle,$$

$$\hat{a}_2(0)|\alpha_2\rangle = \sqrt{\frac{N_a}{2}}|\alpha_2\rangle$$

$$\hat{b}_{02}(t)|\beta_2\rangle = \beta_0|\beta_2\rangle \quad \hat{q}_{2_{in}}(t)|0\rangle = 0|0\rangle, \tag{B5}$$

where we have used again $\hat{b}_{0j}(t) = \hat{b}_j(z_L, t)$ with $j = 1, 2$ for simplicity, and we have considered that $\alpha_1(0) = \alpha_2(0) = \sqrt{N_a/2}$ and $\hat{b}_{01}(t) = \hat{b}_{02}(t) = \beta_0$. Now it is really simple to calculate the atomic expectation values in that case:

$$\langle \hat{N}_{a_1}(t) \rangle = \frac{N_a}{2},$$

$$\langle \hat{N}_{a_1}^2(t) \rangle = \langle \hat{N}_{a_1}^2(t') \rangle = \langle \hat{N}_{a_1}^2(0) \rangle = \frac{N_a}{2} + \frac{N_a^2}{4}. \tag{B6}$$

2. Phase quadrature

The light equation in the case of no spontaneous emission is

$$\hat{b}_1(z_R, t) = \hat{b}_{01}(t)e^{i\frac{g^2}{c\Delta}\hat{a}_1^\dagger(t)\hat{a}_1(t)}. \tag{B7}$$

We select a specific mode of the light field:

$$\hat{\lfloor}_1(\tau) = \frac{\sqrt{c}}{\sqrt{\tau}} \int_0^\tau \hat{b}_1(z_R, t)dt. \tag{B8}$$

Here the atomic population is constant, and thus

$$\hat{\lfloor}_1(\tau) = \frac{\sqrt{c}}{\sqrt{\tau}} e^{i\frac{g^2}{c\Delta}\hat{a}_1^\dagger(t)\hat{a}_1(t)} \int_0^\tau \hat{b}_{01}(t)dt. \tag{B9}$$

We know that the incident light field obeys the following commutation relation: $[\hat{b}_{01}(t), \hat{b}_{01}^\dagger(t')] = \frac{1}{c}\delta(t - t')$. We find the phase quadrature of the specific mode

$$\hat{Y}_1(\tau) \equiv i(\hat{\lfloor}_1(\tau) - \hat{\lfloor}_1^\dagger(\tau))$$

$$= i\frac{\sqrt{c}}{\sqrt{\tau}}\left(e^{i\frac{g^2}{c\Delta}\hat{a}_1^\dagger(t)\hat{a}_1(t)} \int_0^\tau \hat{b}_{01}(t)dt\right.$$

$$\left. - e^{-i\frac{g^2}{c\Delta}\hat{a}_1^\dagger(t)\hat{a}_1(t)} \int_0^\tau \hat{b}_{01}^\dagger(t)dt\right). \tag{B10}$$

We make the small angle approximation

$$\frac{g^2}{c\Delta}\hat{a}_1^\dagger(t)\hat{a}_1(t) \ll 1, \tag{B11}$$

and we get

$$\hat{Y}_1(\tau) \approx \hat{Y}_{1_{\mathrm{in}}}(\tau) - \frac{g^2}{\sqrt{c\tau}\Delta}\hat{a}_1^\dagger(\tau)\hat{a}_1(\tau) \int_0^\tau (\hat{b}_{01}(t) + \hat{b}_{01}^\dagger(t))dt, \tag{B12}$$

where

$$\hat{Y}_{1_{\mathrm{in}}}(\tau) = i\frac{\sqrt{c}}{\sqrt{\tau}} \int_0^\tau (\hat{b}_{01}(t) - \hat{b}_{01}^\dagger(t))dt. \tag{B13}$$

We calculate the expectation value of the phase quadrature

$$\langle \hat{Y}_1(\tau) \rangle \approx -\frac{g^2 N_a \beta_0 \tau}{\Delta\sqrt{c\tau}}, \tag{B14}$$

where we have used that $\langle \hat{Y}_{1_{\mathrm{in}}}(\tau) \rangle = 0$ and assumed that $\beta_0 = \beta_0^*$. We calculate the square of the phase quadrature

$$\hat{Y}_1^2(\tau) \approx \hat{Y}_{1_{\mathrm{in}}}^2(\tau) + \frac{g^4}{c\tau\Delta^2}\hat{a}_1^\dagger(\tau)\hat{a}_1(\tau)\hat{a}_1^\dagger(\tau)\hat{a}_1(\tau) \int_0^\tau \int_0^\tau dt\,dt'$$

$$\times [\hat{b}_{01}(t) + \hat{b}_{01}^\dagger(t)][\hat{b}_{01}(t') + \hat{b}_{01}^\dagger(t')]. \tag{B15}$$

For simplicity we calculate separately

$$Q_1 = \int_0^\tau \int_0^\tau dt\,dt' \,[\hat{b}_{01}(t)\hat{b}_{01}(t') + \hat{b}_{01}(t)\hat{b}_{01}^\dagger(t')$$

$$+ \hat{b}_{01}^\dagger(t)\hat{b}_{01}(t') + \hat{b}_{01}^\dagger(t)\hat{b}_{01}^\dagger(t')]. \tag{B16}$$

After using the commutation relation $[\hat{b}_{01}(t), \hat{b}_{01}^\dagger(t')] = \frac{1}{c}\delta(t - t')$ and the delta function property $\int_0^\tau \delta(t - t')dt' = 1$,

we obtain

$$\langle Q_1 \rangle = 4\beta_0^2 \tau^2 + \frac{\tau}{c}. \tag{B17}$$

Making use of the same commutation relation and the same property of the delta function, we find that $\langle \hat{Y}_{1_{\text{in}}}^2(\tau) \rangle = 1$. Thus,

$$\langle \hat{Y}_1^2(\tau) \rangle \approx 1 + \frac{g^4}{c\tau\Delta^2} \left(\frac{N_a}{2} + \frac{N_a^2}{4} \right) \left(4\beta_0^2\tau^2 + \frac{\tau}{2c} \right), \tag{B18}$$

where we have used Eq. (B6). For simplicity, we can ignore the last term of Eq. (B18) since $4\beta_0^2\tau^2 \gg \tau/2c$:

$$\langle \hat{Y}_1^2(\tau) \rangle \approx 1 + \frac{4g^4\beta_0^2\tau^2}{c\tau\Delta^2} \left(\frac{N_a}{2} + \frac{N_a^2}{4} \right). \tag{B19}$$

From Eq. (B14), we have

$$\langle \hat{Y}_1(\tau) \rangle^2 \approx \frac{g^4\beta_0^2 N_a^2 \tau^2}{c\tau\Delta^2}. \tag{B20}$$

Hence, we finally have

$$\text{Var}(\hat{Y}_1(\tau)) \approx 1 + 2\chi_{\text{ns}}^2 N_a N_{\text{ph}} \tag{B21}$$

and

$$\text{Var}(\hat{S}_b) = 2\text{Var}(\hat{Y}_1(\tau)) \approx 2 + 4\chi_{\text{ns}}^2 N_a N_{\text{ph}}, \tag{B22}$$

where we have defined

$$\chi_{\text{ns}} \equiv \frac{g^2}{c\Delta}, \quad N_{\text{ph}} \equiv \beta_0^2 \tau. \tag{B23}$$

3. Covariances

The covariance of $\hat{J}_z(\tau)$ and $\hat{S}_b(\tau)$ is defined as

$$\text{Cov}(\hat{J}_z(\tau), \hat{S}_b(\tau)) = \langle \hat{J}_z(\tau)\hat{S}_b(\tau) \rangle - \langle \hat{J}_z(\tau) \rangle \langle \hat{S}_b(\tau) \rangle. \tag{B24}$$

We know that $\langle \hat{S}_b(\tau) \rangle = 0$, since $\hat{S}_b = \hat{Y}_2 - \hat{Y}_1$. Hence,

$$\text{Cov}(\hat{J}_z(\tau), \hat{S}_b(\tau)) = \langle \hat{J}_z(\tau)\hat{Y}_2(\tau) \rangle - \langle \hat{J}_z(\tau)\hat{Y}_1(\tau) \rangle. \tag{B25}$$

Using $\hat{J}_z(\tau) = (\hat{N}_{a_1}(\tau) - \hat{N}_{a_2}(\tau))/2$, Eq. (B12) and the atomic expectation values from Appendix B 1, we obtain

$$\text{Cov}(\hat{J}_z(\tau), \hat{S}_b(\tau)) \approx \chi_{\text{ns}} N_a \sqrt{N_{\text{ph}}}. \tag{B26}$$

4. Quantum enhancement parameter ξ_s

Inserting Eqs. (B26) and (B22) into (A5), we obtain

$$\text{Var}(\hat{S}_2(\tau)) \approx \frac{N_a}{4} \left(1 - \frac{\chi_{\text{ns}}^2 N_{\text{ph}} N_a}{\chi_{\text{ns}}^2 N_{\text{ph}} N_a + 1/2} \right). \tag{B27}$$

Using the atomic equations of motion, we find for small exponents $\chi_{\text{ns}}^2 N_{\text{ph}} \ll 1$

$$\langle \hat{J}_x(\tau) \rangle \approx \frac{N_a}{2} e^{-\chi_{\text{ns}}^2 N_{\text{ph}}}. \tag{B28}$$

Finally, from Eq. (A6) we obtain

$$\xi_{s_2}^{ns}(\tau) \approx e^{\chi_{\text{ns}}^2 N_{\text{ph}}} \left(1 - \frac{\chi_{\text{ns}}^2 N_{\text{ph}} N_a}{\chi_{\text{ns}}^2 N_{\text{ph}} N_a + 1/2} \right)^{1/2}. \tag{B29}$$

APPENDIX C: SPONTANEOUS EMISSION

1. Atomic expectation values

In the case where we have incorporated spontaneous emission, the calculation of the atomic expectation values is more complicated, since we use the following atomic equations:

$$\hat{a}_1(t) = \hat{a}_1(0) e^{ig^2(\Omega + i\Gamma) \int_0^t \hat{b}_{01}^\dagger(t')\hat{b}_{01}(t')dt'}$$
$$+ \frac{g\sqrt{\gamma_3}}{\Delta - i\gamma_3/2} e^{ig^2(\Omega + i\Gamma) \int_0^t \hat{b}_{01}^\dagger(t')\hat{b}_{01}(t')dt'} \int_0^t dt' \hat{b}_{01}^\dagger(t')\hat{q}_{1_{\text{in}}}(t') e^{-ig^2(\Omega + i\Gamma) \int_0^{t'} \hat{b}_{01}^\dagger(t'')\hat{b}_{01}(t'')dt''} \tag{C1a}$$

$$\hat{a}_1^\dagger(t) = \hat{a}_1^\dagger(0) e^{-ig^2(\Omega - i\Gamma) \int_0^t \hat{b}_{01}^\dagger(t')\hat{b}_{01}(t')dt'}$$
$$+ \frac{g\sqrt{\gamma_3}}{\Delta + i\gamma_3/2} e^{-ig^2(\Omega - i\Gamma) \int_0^t \hat{b}_{01}^\dagger(t')\hat{b}_{01}(t')dt'} \int_0^t dt' \hat{b}_{01}(t')\hat{q}_{1_{\text{in}}}^\dagger(t') e^{ig^2(\Omega - i\Gamma) \int_0^{t'} \hat{b}_{01}^\dagger(t'')\hat{b}_{01}(t'')dt''}. \tag{C1b}$$

For simplicity, we assume that the intensity operator in the exponentials does not depend on time; namely, it is a constant number $\hat{b}_{01}^\dagger(t)\hat{b}_{01}(t) \approx \beta_0^2$. We essentially assume here that the atomic loss is due to the average field intensity. We also ignore the unitary part of the exponentials, since they would cancel out during the calculation of the atomic expectation values. So, we finally have

$$\hat{a}_1(t) = \underbrace{\sqrt{\epsilon(t)}\hat{a}_1(0)}_{\hat{A}_1(t)} + \underbrace{\frac{g\sqrt{\gamma_3}}{\Delta - i\gamma_3/2}\sqrt{\epsilon(t)} \int_0^t \sqrt{\epsilon^{-1}(t')}\hat{b}_{01}^\dagger(t')\hat{q}_{1_{\text{in}}}(t')dt'}_{\hat{A}_2(t)}, \tag{C2}$$

$$\hat{a}_1^\dagger(t) = \underbrace{\sqrt{\epsilon(t)}\hat{a}_1^\dagger(0)}_{\hat{A}_1^\dagger(t)} + \underbrace{\frac{g\sqrt{\gamma_3}}{\Delta + i\gamma_3/2}\sqrt{\epsilon(t)} \int_0^t \sqrt{\epsilon^{-1}(t')}\hat{b}_{01}(t')\hat{q}_{1_{\text{in}}}^\dagger(t')dt'}_{\hat{A}_2^\dagger(t)}, \tag{C3}$$

where we have defined

$$\epsilon(t) \equiv e^{-2g^2\Gamma\beta_0^2 t}. \tag{C4}$$

We calculate the expectation value of atoms in state $|1\rangle$,

$$\langle \hat{N}_{a_1}(t)\rangle = \langle \hat{a}_1^\dagger(t)\hat{a}_1(t)\rangle = \frac{N_a}{2}\epsilon(t), \tag{C5}$$

where $\epsilon(t)$ indicates the atomic rate of loss in our system at time t. Now we are going to calculate the more complicated expectation value $\langle \hat{N}_{a_1}(t)\hat{N}_{a_1}(t')\rangle$. We have named all terms of Eqs. (C2) and (C3) for simplicity, in order to clearly show which terms finally survive:

$$\langle \hat{N}_{a_1}(t)\hat{N}_{a_1}(t')\rangle = \langle \hat{A}_1^\dagger(t)\hat{A}_1(t)\hat{A}_1^\dagger(t')\hat{A}_1(t')\rangle + \langle \hat{A}_1^\dagger(t)\hat{A}_2(t)\hat{A}_2^\dagger(t')\hat{A}_1(t')\rangle, \tag{C6}$$

where all the other terms in this product are zero since $\langle \hat{q}_{1_{\mathrm{in}}}\rangle = \langle \hat{q}_{1_{\mathrm{in}}}^\dagger\rangle = \langle \hat{q}_{1_{\mathrm{in}}}^\dagger \hat{q}_{1_{\mathrm{in}}}\rangle = 0$. The first term of the above equation is easily calculated:

$$\langle \hat{A}_1^\dagger(t)\hat{A}_1(t)\hat{A}_1^\dagger(t')\hat{A}_1(t')\rangle = \left(\frac{N_a}{2} + \frac{N_a^2}{4}\right)\epsilon(t)\epsilon(t'). \tag{C7}$$

However, the second term is more complicated:

$$\langle \hat{A}_1^\dagger(t)\hat{A}_2(t)\hat{A}_2^\dagger(t')\hat{A}_1(t')\rangle = 2g^2\Gamma\epsilon(t)\epsilon(t')\langle \hat{a}_1^\dagger(0)\hat{a}_1(0)\rangle$$
$$\times \int_0^t \int_0^{t'} d\xi\, ds\, \sqrt{\epsilon^{-1}(s)}\sqrt{\epsilon^{-1}(\xi)}\langle \hat{b}_{01}^\dagger(s)\hat{b}_{01}(\xi)\rangle\langle \hat{q}_{1_{\mathrm{in}}}(s)\hat{q}_{1_{\mathrm{in}}}^\dagger(\xi)\rangle. \tag{C8}$$

We use the commutation relation for the temporal part of the Langevin noise:

$$[\hat{q}_{1_{\mathrm{in}}}(s), \hat{q}_{1_{\mathrm{in}}}^\dagger(\xi)] = \delta(\xi - s). \tag{C9}$$

We also make use of the following property of the delta function,

$$\int_0^{t'} d\xi\, f(\xi)\delta(\xi - s) = f(s)\Theta(t' - s), \tag{C10}$$

where $\Theta(t' - s)$ is the Heaviside step function, and using $\langle \hat{b}_{01}^\dagger(s)\hat{b}_{01}(s)\rangle = \beta_0^2$ we obtain

$$\langle \hat{A}_1^\dagger(t)\hat{A}_2(t)\hat{A}_2^\dagger(t')\hat{A}_1(t')\rangle$$
$$= g^2\Gamma N_a\beta_0^2\epsilon(t)\epsilon(t')\int_0^t ds\, \epsilon^{-1}(s)\Theta(t' - s). \tag{C11}$$

For $t \geqslant t'$, we have

$$\langle \hat{A}_1^\dagger(t)\hat{A}_2(t)\hat{A}_2^\dagger(t')\hat{A}_1(t')\rangle = \frac{N_a}{2}\epsilon(t)[1 - \epsilon(t')], \tag{C12}$$

and using Eqs. (C6), (C7) and (C12) we get

$$\langle \hat{N}_{a_1}(t)\hat{N}_{a_1}(t')\rangle = \frac{N_a^2}{4}\epsilon(t)\epsilon(t') + \frac{N_a}{2}\epsilon(t), \tag{C13}$$

while for $t < t'$ we have

$$\langle \hat{A}_1^\dagger(t)\hat{A}_2(t)\hat{A}_2^\dagger(t')\hat{A}_1(t')\rangle = \frac{N_a}{2}\epsilon(t')[1 - \epsilon(t)] \tag{C14}$$

and

$$\langle \hat{N}_{a_1}(t)\hat{N}_{a_1}(t')\rangle = \frac{N_a^2}{4}\epsilon(t)\epsilon(t') + \frac{N_a}{2}\epsilon(t'). \tag{C15}$$

We notice that we obtain the same result for the double integral with respect to t and t' for both cases, $t \geqslant t'$ and for

$t < t'$,

$$\int_0^\tau \int_0^\tau dt\, dt'\, \langle \hat{N}_{a_1}(t)\hat{N}_{a_1}(t')\rangle = \frac{N_a^2}{4}I_1^2 + \frac{N_a}{2}I_1\tau, \tag{C16}$$

but distinguishing between the two cases would be important when we calculate the covariance of $\hat{J}_z(\tau)$ and $\hat{S}_b(\tau)$. For simplicity, we have also defined

$$I_1(\tau) \equiv \int_0^\tau dt\, \epsilon(t) = \frac{1 - \epsilon(\tau)}{2g^2\Gamma\beta_0^2}. \tag{C17}$$

We can now calculate

$$\int_0^\tau dt\langle \hat{N}_{a_1}(t)\rangle = \frac{N_a}{2}I_1. \tag{C18}$$

2. Phase quadrature

In the case of spontaneous emission, the photon operator is given by the following equation:

$$\hat{b}_1(z_R, t) = \hat{b}_{01}(t)e^{i\frac{g^2}{c}(\Omega + i\Gamma)\hat{a}_1^\dagger(t)\hat{a}_1(t)}$$
$$+ \frac{g}{c}\frac{\sqrt{\gamma_3}}{\Delta - i\gamma_3/2}\hat{a}_1^\dagger(t)\hat{q}_{1_{\mathrm{in}}}(t). \tag{C19}$$

Again, we define the phase quadrature operator of a specific mode of the light field

$$\hat{Y}_1(\tau) = i(\hat{\mathsf{l}}_1(\tau) - \hat{\mathsf{l}}_1^\dagger(\tau)), \tag{C20}$$

where

$$\hat{\mathsf{l}}_1(t) = \frac{\sqrt{c}}{\sqrt{\tau}}\int_0^\tau \hat{b}_{01}(t)dt. \tag{C21}$$

Making the small angle approximation $g^2(\Omega + i\Gamma)\hat{a}_1^\dagger\hat{a}_1/c \ll 1$, we obtain

$$\hat{Y}_1 \approx \hat{Y}_{1_{\mathrm{in}}} - \frac{g^2\Omega}{\sqrt{c\tau}}\int_0^\tau (\hat{b}_{01}(t) + \hat{b}_{01}^\dagger(t))\hat{a}_1^\dagger(t)\hat{a}_1(t)dt$$
$$- \frac{g^2\Gamma}{\sqrt{c\tau}}\int_0^\tau (\hat{b}_{01}(t) - \hat{b}_{01}^\dagger(t))\hat{a}_1^\dagger(t)\hat{a}_1(t)dt$$

$$+ i \frac{g\Omega\sqrt{\gamma_3}}{\sqrt{c\tau}} \int_0^\tau dt \left(\hat{q}_{1_{\text{in}}}(t)\hat{a}_1^\dagger(t) - \hat{q}_{1_{\text{in}}}^\dagger(t)\hat{a}_1(t) \right)$$

$$- i \frac{g\Gamma\sqrt{\gamma_3}}{\sqrt{c\tau}} \int_0^\tau dt \left(\hat{q}_{1_{\text{in}}}(t)\hat{a}_1^\dagger(t) + \hat{q}_{1_{\text{in}}}^\dagger(t)\hat{a}_1(t) \right), \quad \text{(C22)}$$

where

$$\hat{Y}_{1_{\text{in}}}(\tau) \equiv i \frac{\sqrt{c}}{\sqrt{\tau}} \int_0^\tau dt \left(\hat{b}_{01}(t) - \hat{b}_{01}^\dagger(t) \right). \quad \text{(C23)}$$

We calculate the expectation value of $\hat{Y}_1(\tau)$

$$\langle \hat{Y}_1(\tau) \rangle \approx -\frac{2\beta_0 \Omega g^2}{\sqrt{c\tau}} \int_0^\tau dt \langle \hat{N}_{a_1}(t) \rangle. \quad \text{(C24)}$$

From Eq. (C18), we get

$$\langle \hat{Y}_1 \rangle^2 \approx \frac{g^4 \Omega^2 \beta_0^2 N_a^2 I_1^2}{c\tau}. \quad \text{(C25)}$$

Now we are going to calculate $\langle \hat{Y}_1^2 \rangle$, where for simplicity we keep only the terms coming from the the first two terms of Eq. (C22), since they are the dominant terms:

$$\langle \hat{Y}_1^2 \rangle \approx 1 + \frac{4g^4 \Omega^2}{c\tau} \beta_0^2 \int_0^\tau \int_0^\tau dt\,dt' \langle \hat{N}_{a_1}(t')\hat{N}_{a_1}(t) \rangle. \quad \text{(C26)}$$

Substituting Eq. (C16) in (C26) and using (C25), we obtain

$$\text{Var}(\hat{Y}_1(\tau)) \approx 1 + 2\chi_1^2 N_{\text{ph}} N_a \overline{\epsilon(\tau)}, \quad \text{(C27)}$$

where we have defined $\chi_1 \equiv \frac{g^2\Omega}{c}$ and $\overline{\epsilon(\tau)} = \frac{1}{\tau} \int_0^\tau \epsilon(t)dt$, which is the time average of the decay. We notice that $\chi_1 = \chi_{\text{ns}}$ in the no spontaneous emission case ($\gamma_3 = 0$). As we mentioned before, $\text{Var}(\hat{S}_b) = 2\text{Var}(\hat{Y}_1)$, and thus

$$\text{Var}(\hat{S}_b(\tau)) \approx 2 + 4\chi_1^2 N_{\text{ph}} N_a \overline{\epsilon(\tau)}. \quad \text{(C28)}$$

3. Covariances

The covariance of $\hat{J}_z$ and $\hat{S}_b$ is again given by $\text{Cov}(\hat{J}_z(\tau), \hat{S}_b(\tau)) = \langle \hat{J}_z(\tau)\hat{Y}_2(\tau) \rangle - \langle \hat{J}_z(\tau)\hat{Y}_1(\tau) \rangle$, which gives

$$\text{Cov}(\hat{J}_z(\tau), \hat{S}_b(\tau))$$
$$= \frac{2g^2\Omega\beta_0}{\sqrt{c\tau}} \int_0^\tau dt \left(\langle \hat{N}_{a_1}(\tau)\hat{N}_{a_1}(t) \rangle - \langle \hat{N}_{a_1}(\tau)\hat{N}_{a_2}(t) \rangle \right), \quad \text{(C29)}$$

since

$$\langle \hat{N}_{a_1}(\tau)\hat{N}_{a_1}(t) \rangle = \langle \hat{N}_{a_2}(\tau)\hat{N}_{a_2}(t) \rangle,$$
$$\langle \hat{N}_{a_1}(\tau)\hat{N}_{a_2}(t) \rangle = \langle \hat{N}_{a_2}(\tau)\hat{N}_{a_1}(t) \rangle. \quad \text{(C30)}$$

Now we have to be a bit more careful, compared to the no spontaneous emission case, because we have two different expressions for $\langle \hat{N}_{a_1}(t)\hat{N}_{a_1}(t') \rangle$ depending on whether $t \geqslant t'$ or $t < t'$. That is why we are going to calculate $\text{Cov}(\hat{S}_b(\tau), \hat{J}_z(\tau))$ as well:

$$\text{Cov}(\hat{S}_b(\tau), \hat{J}_z(\tau))$$
$$= \frac{2g^2\Omega\beta_0}{\sqrt{c\tau}} \int_0^\tau dt \left(\langle \hat{N}_{a_1}(t)\hat{N}_{a_1}(\tau) \rangle - \langle \hat{N}_{a_1}(t)\hat{N}_{a_2}(\tau) \rangle \right). \quad \text{(C31)}$$

For the first covariance, where $\tau \geqslant t$, we use Eq. (C13), and hence

$$\int_0^\tau dt \langle \hat{N}_{a_1}(\tau)\hat{N}_{a_1}(t) \rangle = \frac{N_a^2}{4}\epsilon(\tau)I_1 + \frac{N_a}{2}\epsilon(\tau)\tau. \quad \text{(C32)}$$

We calculate the simpler term

$$\langle \hat{N}_{a_1}(\tau)\hat{N}_{a_2}(t) \rangle = \frac{N_a^2}{4}\epsilon(\tau)\epsilon(t), \quad \text{(C33)}$$

since $\hat{a}_1(t)$ commutes with $\hat{a}_2(t')$ for all t and t'. Thus,

$$\int_0^\tau dt \langle \hat{N}_{a_1}(\tau)\hat{N}_{a_2}(t) \rangle = \frac{N_a^2}{4}\epsilon(\tau)I_1. \quad \text{(C34)}$$

We finally have

$$\text{Cov}(\hat{J}_z(\tau), \hat{S}_b(\tau)) = \chi_1\sqrt{N_{\text{ph}}}N_a\epsilon(\tau), \quad \text{(C35)}$$

where we used again $\chi = \frac{g^2\Omega}{c}$. For the second covariance, we use Eq. (C15) for $t < t'$ and we obtain

$$\int_0^\tau dt \langle \hat{N}_{a_1}(t)\hat{N}_{a_1}(\tau) \rangle = \frac{N_a^2}{4}\epsilon(\tau)I_1 + \frac{N_a}{2}\epsilon(\tau)\tau, \quad \text{(C36)}$$

$$\int_0^\tau dt \langle \hat{N}_{a_1}(t)\hat{N}_{a_2}(\tau) \rangle = \frac{N_a^2}{4}\epsilon(\tau)I_1. \quad \text{(C37)}$$

Hence, we finally get the same result for both covariances as we expected:

$$\text{Cov}(\hat{J}_z(\tau), \hat{S}_b(\tau)) = \text{Cov}(\hat{S}_b(\tau), \hat{J}_z(\tau)) = \chi_1\sqrt{N_{\text{ph}}}N_a\epsilon(\tau). \quad \text{(C38)}$$

4. Quantum enhancement parameter ξ_s

Substituting Eqs. (C28) and (C38) into Eq. (A5), we get

$$\text{Var}(\hat{S}_2(\tau)) \approx \frac{N_a}{4}\epsilon(\tau)\left(1 - \frac{\chi_1^2 N_{\text{ph}} N_a \epsilon(\tau)}{\chi_1^2 N_{\text{ph}} N_a \overline{\epsilon(\tau)} + 1/2} \right). \quad \text{(C39)}$$

Using the atomic equations, we find the expectation value of $\hat{J}_x$ for $(\chi_1^2 + 2\chi_2)N_{\text{ph}} \ll 1$,

$$\langle \hat{J}_x(t) \rangle \approx \frac{N_a}{2} e^{-(\chi_1^2 + 2\chi_2)N_{\text{ph}}}, \quad \text{(C40)}$$

where we have defined $\chi_2 \equiv g^2\Gamma/c$. Now we can express $\epsilon(\tau)$ in a more convenient way: $\epsilon(\tau) = e^{-2\chi_2 N_{\text{ph}}}$. Finally, the squeezing parameter is given by

$$\xi_{s_2} \approx e^{(\chi_1^2 + \chi_2)N_{\text{ph}}} \left(1 - \frac{\chi_1^2 N_{\text{ph}} N_a \epsilon(\tau)}{\chi_1^2 N_{\text{ph}} N_a \overline{\epsilon(\tau)} + 1/2} \right)^{1/2}, \quad \text{(C41)}$$

where for convenience we present again all the parameter definitions we made throughout this calculation:

$$\chi_1 \equiv \frac{g^2\Omega}{c}, \quad \chi_2 \equiv \frac{g^2\Gamma}{c},$$

$$\overline{\epsilon(\tau)} \equiv \frac{1}{\tau} \int_0^\tau \epsilon(t)dt, \quad \epsilon(\tau) = e^{-2\chi_2 N_{\text{ph}}}. \quad \text{(C42)}$$

[1] A. D. Cronin, J. Schmiedmayer, and D. E. Pritchard, Optics and interferometry with atoms and molecules, Rev. Mod. Phys. **81**, 1051 (2009).

[2] N. P. Robins, P. A. Altin, J. E. Debs, and J. D. Close, Atom lasers: Production, properties, and prospects for precision inertial measurement, Phys. Rep. **529**, 265 (2013).

[3] M. Johnsson, S. Haine, J. Hope, N. Robins, C. Figl, M. Jeppesen, J. Dugué, and J. Close, Semiclassical limits to the linewidth of an atom laser, Phys. Rev. A **75**, 043618 (2007).

[4] J. E. Debs, P. A. Altin, T. H. Barter, D. Döring, G. R. Dennis, G. McDonald, R. P. Anderson, J. D. Close, and N. P. Robins, Cold-atom gravimetry with a Bose-Einstein condensate, Phys. Rev. A **84**, 033610 (2011).

[5] S. S. Szigeti, J. E. Debs, J. J. Hope, N. P. Robins, and J. D. Close, Why momentum width matters for atom interferometry with Bragg pulses, New J. Phys. **14**, 023009 (2012).

[6] G. D. McDonald, C. C. N. Kuhn, S. Bennetts, J. E. Debs, K. S. Hardman, M. Johnsson, J. D. Close, and N. P. Robins, $80\hbar k$ momentum separation with Bloch oscillations in an optically guided atom interferometer, Phys. Rev. A **88**, 053620 (2013).

[7] M. Kritsotakis, S. S. Szigeti, J. A. Dunningham, and S. A. Haine, Optimal matter-wave gravimetry, Phys. Rev. A **98**, 023629 (2018).

[8] D. J. Wineland, J. J. Bollinger, W. M. Itano, F. L. Moore, and D. J. Heinzen, Spin squeezing and reduced quantum noise in spectroscopy, Phys. Rev. A **46**, R6797 (1992).

[9] M. Kitagawa and M. Ueda, Squeezed spin states, Phys. Rev. A **47**, 5138 (1993).

[10] A. S. Sørensen and K. Mølmer, Entanglement And Extreme Spin Squeezing, Phys. Rev. Lett. **86**, 4431 (2001).

[11] L. Pezzè, A. Smerzi, M. K. Oberthaler, R. Schmied, and P. Treutlein, Quantum metrology with nonclassical states of atomic ensembles, Rev. Mod. Phys. **90**, 035005 (2018).

[12] L.-M. Duan, A. Sørensen, J. I. Cirac, and P. Zoller, Squeezing And Entanglement of Atomic Beams, Phys. Rev. Lett. **85**, 3991 (2000).

[13] H. Pu and P. Meystre, Creating Macroscopic Atomic Einstein-Podolsky-Rosen States from Bose-Einstein Condensates, Phys. Rev. Lett. **85**, 3987 (2000).

[14] A. Søndberg Sørensen, Bogoliubov theory of entanglement in a Bose-Einstein condensate, Phys. Rev. A **65**, 043610 (2002).

[15] A. Micheli, D. Jaksch, J. I. Cirac, and P. Zoller, Many-particle entanglement in two-component Bose-Einstein condensates, Phys. Rev. A **67**, 013607 (2003).

[16] K. V. Kheruntsyan, M. K. Olsen, and P. D. Drummond, Einstein-Podolsky-Rosen Correlations Via Dissociation of a Molecular Bose-Einstein Condensate, Phys. Rev. Lett. **95**, 150405 (2005).

[17] M. T. Johnsson and S. A. Haine, Generating Quadrature Squeezing in an Atom Laser Through Self-Interaction, Phys. Rev. Lett. **99**, 010401 (2007).

[18] Y. Li, P. Treutlein, J. Reichel, and A. Sinatra, Spin squeezing in a bimodal condensate: Spatial dynamics and particle losses, Eur. Phys. J. B **68**, 365 (2009).

[19] S. S. Mirkhalaf, S. P. Nolan, and S. A. Haine, Robustifying twist-and-turn entanglement with interaction-based readout, Phys. Rev. A **97**, 053618 (2018).

[20] A. Kuzmich, K. Mølmer, and E. S. Polzik, Spin Squeezing in an Ensemble of Atoms Illuminated with Squeezed Light, Phys. Rev. Lett. **79**, 4782 (1997).

[21] A. Kuzmich, N. P. Bigelow, and L. Mandel, Atomic quantum non-demolition measurements and squeezing, EPL **42**, 481 (1998).

[22] M. G. Moore, O. Zobay, and P. Meystre, Quantum optics of a Bose-Einstein condensate coupled to a quantized light field, Phys. Rev. A **60**, 1491 (1999).

[23] A. Kuzmich, L. Mandel, and N. P. Bigelow, Generation of Spin Squeezing Via Continuous Quantum Nondemolition Measurement, Phys. Rev. Lett. **85**, 1594 (2000).

[24] H. Jing, J.-L. Chen, and M.-L. Ge, Quantum-dynamical theory for squeezing the output of a Bose-Einstein condensate, Phys. Rev. A **63**, 015601 (2000).

[25] M. Fleischhauer and S. Gong, Stationary Source of Nonclassical or Entangled Atoms, Phys. Rev. Lett. **88**, 070404 (2002).

[26] S. A. Haine and J. J. Hope, Outcoupling from a Bose-Einstein condensate with squeezed light to produce entangled-atom laser beams, Phys. Rev. A **72**, 033601 (2005).

[27] S. A. Haine and J. J. Hope, A multi-mode model of a non-classical atom laser produced by outcoupling from a Bose-Einstein condensate with squeezed light, Laser Phys. Lett. **2**, 597 (2005).

[28] S. R. de Echaniz, M. W. Mitchell, M. Kubasik, M. Koschorreck, H. Crepaz, J. Eschner, and E. S. Polzik, Conditions for spin squeezing in a cold ^{87}Rb ensemble, J. Opt. B: Quantum Semiclassical Opt. **7**, S548 (2005).

[29] S. A. Haine, M. K. Olsen, and J. J. Hope, Generating Controllable Atom-Light Entanglement with a Raman Atom Laser System, Phys. Rev. Lett. **96**, 133601 (2006).

[30] K. Hammerer, A. S. Sørensen, and E. S. Polzik, Quantum interface between light and atomic ensembles, Rev. Mod. Phys. **82**, 1041 (2010).

[31] S. A. Haine, Information-Recycling Beam Splitters for Quantum Enhanced Atom Interferometry, Phys. Rev. Lett. **110**, 053002 (2013).

[32] G. Puentes, G. Colangelo, R. J. Sewell, and M. W. Mitchell, Planar squeezing by quantum non-demolition measurement in cold atomic ensembles, New J. Phys. **15**, 103031 (2013).

[33] S. S. Szigeti, B. Tonekaboni, W. Y. S. Lau, S. N. Hood, and S. A. Haine, Squeezed-light-enhanced atom interferometry below the standard quantum limit, Phys. Rev. A **90**, 063630 (2014).

[34] B. Tonekaboni, S. A. Haine, and S. S. Szigeti, Heisenberg-limited metrology with a squeezed vacuum state, three-mode mixing, and information recycling, Phys. Rev. A **91**, 033616 (2015).

[35] S. A. Haine, S. S. Szigeti, M. D. Lang, and C. M. Caves, Heisenberg-limited metrology with information recycling, Phys. Rev. A **91**, 041802(R) (2015).

[36] S. A. Haine and S. S. Szigeti, Quantum metrology with mixed states: When recovering lost information is better than never losing it, Phys. Rev. A **92**, 032317 (2015).

[37] S. A. Haine and W. Y. S. Lau, Generation of atom-light entanglement in an optical cavity for quantum enhanced atom interferometry, Phys. Rev. A **93**, 023607 (2016).

[38] L. Salvi, N. Poli, V. Vuletić, and G. M. Tino, Squeezing on Momentum States for Atom Interferometry, Phys. Rev. Lett. **120**, 033601 (2018).

[39] J. Esteve, C. Gross, A. Weller, S. Giovanazzi, and M. K. Oberthaler, Squeezing and entanglement in a Bose-Einstein condensate, Nature (London) **455**, 1216 (2008).

[40] C. Gross, T. Zibold, E. Nicklas, J. Esteve, and M. K. Oberthaler, Nonlinear atom interferometer surpasses classical precision limit, Nature (London) **464**, 1165 (2010).

[41] M. F. Riedel, P. Böhi, Y. Li, T. W. Hänsch, A. Sinatra, and P. Treutlein, Atom-chip-based generation of entanglement for quantum metrology, Nature (London) **464**, 1170 (2010).

[42] B. Lücke, M. Scherer, J. Kruse, L. Pezze, F. Deuretzbacher, P. Hyllus, O. Topic, J. Peise, W. Ertmer, J. Arlt, L. Santos, A. Smerzi, and C. Klempt, Twin matter waves for interferometry beyond the classical limit, Science **334**, 773 (2011).

[43] C. D. Hamley, C. S. Gerving, T. M. Hoang, E. M. Bookjans, and M. S. Chapman, Spin-nematic squeezed vacuum in a quantum gas, Nat. Phys. **8**, 305 (2012).

[44] H. Strobel, W. Muessel, D. Linnemann, T. Zibold, D. B. Hume, L. Pezzè, A. Smerzi, and M. K. Oberthaler, Fisher information and entanglement of non-Gaussian spin states, Science **345**, 424 (2014).

[45] W. Muessel, H. Strobel, D. Linnemann, D. B. Hume, and M. K. Oberthaler, Scalable Spin Squeezing for Quantum-Enhanced Magnetometry with Bose-Einstein Condensates, Phys. Rev. Lett. **113**, 103004 (2014).

[46] I. Kruse, K. Lange, J. Peise, B. Lücke, L. Pezzè, J. Arlt, W. Ertmer, C. Lisdat, L. Santos, A. Smerzi, and C. Klempt, Improvement of an Atomic Clock Using Squeezed Vacuum, Phys. Rev. Lett. **117**, 143004 (2016).

[47] D. Linnemann, H. Strobel, W. Muessel, J. Schulz, R. J. Lewis-Swan, K. V. Kheruntsyan, and M. K. Oberthaler, Quantum-Enhanced Sensing Based on Time Reversal of Nonlinear Dynamics, Phys. Rev. Lett. **117**, 013001 (2016).

[48] Y.-Q. Zou, L.-N. Wu, Q. Liu, X.-Y. Luo, S.-F. Guo, J.-H. Cao, M. K. Tey, and L. You, Beating the classical precision limit with spin-1 Dicke states of more than 10,000 atoms, Proc. Natl. Acad. Sci. U.S.A. **115**, 6381 (2018).

[49] S. A. Haine and M. T. Johnsson, Dynamic scheme for generating number squeezing in Bose-Einstein condensates through nonlinear interactions, Phys. Rev. A **80**, 023611 (2009).

[50] S. A. Haine and A. J. Ferris, Surpassing the standard quantum limit in an atom interferometer with four-mode entanglement produced from four-wave mixing, Phys. Rev. A **84**, 043624 (2011).

[51] B. Opanchuk, M. Egorov, S. Hoffmann, A. I. Sidorov, and P. D. Drummond, Quantum noise in three-dimensional BEC interferometry, EPL **97**, 50003 (2012).

[52] S. A. Haine, J. Lau, R. P. Anderson, and M. T. Johnsson, Self-induced spatial dynamics to enhance spin squeezing via one-axis twisting in a two-component Bose-Einstein condensate, Phys. Rev. A **90**, 023613 (2014).

[53] S. P. Nolan, J. Sabbatini, M. W. J. Bromley, M. J. Davis, and S. A. Haine, Quantum enhanced measurement of rotations with a spin-1 Bose-Einstein condensate in a ring trap, Phys. Rev. A **93**, 023616 (2016).

[54] S. A. Haine, Quantum noise in bright soliton matter-wave interferometry, New J. Phys. **20**, 033009 (2018).

[55] J. Appel, P. J. Windpassinger, D. Oblak, U. B. Hoff, N. Kjaergaard, and E. S. Polzik, Mesoscopic atomic entanglement for precision measurements beyond the standard quantum limit, Proc. Natl. Acad. Sci. U.S.A. **106**, 10960 (2009).

[56] A. Louchet-Chauvet, J. Appel, J. J. Renema, D. Oblak, N. Kjaergaard, and E. S. Polzik, Entanglement-assisted atomic clock beyond the projection noise limit, New J. Phys. **12**, 065032 (2010).

[57] M. H. Schleier-Smith, I. D. Leroux, and V. Vuletić, Squeezing the collective spin of a dilute atomic ensemble by cavity feedback, Phys. Rev. A **81**, 021804(R) (2010).

[58] M. H. Schleier-Smith, I. D. Leroux, and V. Vuletić, States of an Ensemble of Two-Level Atoms with Reduced Quantum Uncertainty, Phys. Rev. Lett. **104**, 073604 (2010).

[59] I. D. Leroux, M. H. Schleier-Smith, and V. Vuletić, Implementation of Cavity Squeezing of a Collective Atomic Spin, Phys. Rev. Lett. **104**, 073602 (2010).

[60] M. Koschorreck, M. Napolitano, B. Dubost, and M. W. Mitchell, Quantum Nondemolition Measurement of Large-Spin Ensembles by Dynamical Decoupling, Phys. Rev. Lett. **105**, 093602 (2010).

[61] R. J. Sewell, M. Koschorreck, M. Napolitano, B. Dubost, N. Behbood, and M. W. Mitchell, Magnetic Sensitivity Beyond the Projection Noise Limit by Spin Squeezing, Phys. Rev. Lett. **109**, 253605 (2012).

[62] R. J. Sewell, M. Napolitano, N. Behbood, G. Colangelo, F. Martin Ciurana, and M. W. Mitchell, Ultrasensitive Atomic Spin Measurements with a Nonlinear Interferometer, Phys. Rev. X **4**, 021045 (2014).

[63] O. Hosten, N. J. Engelsen, R. Krishnakumar, and M. A. Kasevich, Measurement noise 100 times lower than the quantum-projection limit using entangled atoms, Nature (London) **529**, 505 (2016).

[64] P. A. Altin, M. T. Johnsson, V. Negnevitsky, G. R. Dennis, R. P. Anderson, J. E. Debs, S. S. Szigeti, K. S. Hardman, S. Bennetts, G. D. McDonald, L. D. Turner, J. D. Close, and N. P. Robins, Precision atomic gravimeter based on Bragg diffraction, New J. Phys. **15**, 023009 (2013).

[65] M. Kasevich and S. Chu, Measurement of the gravitational acceleration of an atom with a light-pulse atom interferometer, Appl. Phys. B: Lasers Optics **54**, 321 (1992).

[66] F. Riehle, T. Kisters, A. Witte, J. Helmcke, and C. J. Bordé, Optical Ramsey Spectroscopy in a Rotating Frame: Sagnac Effect in a Matter-Wave Interferometer, Phys. Rev. Lett. **67**, 177 (1991).

[67] W. P. Schleich, D. M. Greenberger, and E. M. Rasel, Redshift Controversy in Atom Interferometry: Representation Dependence of the Origin of Phase Shift, Phys. Rev. Lett. **110**, 010401 (2013).

[68] S. Kleinert, E. Kajari, A. Roura, and W. P. Schleich, Representation-free description of light-pulse atom interferometry including non-inertial effects, Phys. Rep. **605**, 1 (2015).

[69] A. Bertoldi, F. Minardi, and M. Prevedelli, Phase shift in atom interferometers: Corrections for nonquadratic potentials and finite-duration laser pulses, Phys. Rev. A **99**, 033619 (2019).

[70] J. M. Radcliffe, Some properties of coherent spin states, J. Phys. A: Gen. Phys. **4**, 313 (1971).

[71] S. S. Szigeti, S. P. Nolan, J. D. Close, and S. A. Haine, High-Precision Quantum-Enhanced Gravimetry with a Bose-Einstein Condensate, Phys. Rev. Lett. **125**, 100402 (2020).

[72] C. W. Gardiner and M. J. Collett, Input and output in damped quantum systems: Quantum stochastic differential equations and the master equation, Phys. Rev. A **31**, 3761 (1985).

[73] E. Brion, L. H. Pedersen, and K. Mølmer, Adiabatic elimination in a lambda system, J. Phys. A: Math. Theor. **40**, 1033 (2007).

[74] H. A. Bachor and T. C. Ralph, *A Guide to Experiments in Quantum Optics*, 2nd ed. (Wiley, New York, 2004).

[75] L.-M. Duan, J. I. Cirac, P. Zoller, and E. S. Polzik, Quantum Communication Between Atomic Ensembles Using Coherent Light, Phys. Rev. Lett. **85**, 5643 (2000).

[76] L. B. Madsen and K. Mølmer, Spin squeezing and precision probing with light and samples of atoms in the Gaussian description, Phys. Rev. A **70**, 052324 (2004).

[77] C. Gardiner and P. Zoller, *Quantum Noise: A Handbook of Markovian and non-Markovian Quantum Stochastic Methods with Applications to Quantum Optics*, Springer Series in Synergetics, Vol. 56 (Springer Science & Business Media, Berlin, 2004).

[78] D. A. Steck, Rubidium 87 d line data, revision 2.1.5 (2015), https://steck.us/alkalidata/rubidium87numbers.pdf.

[79] K. M. Mertes, J. W. Merrill, R. Carretero-González, D. J. Frantzeskakis, P. G. Kevrekidis, and D. S. Hall, Nonequilibrium Dynamics and Superfluid Ring Excitations in Binary Bose-Einstein Condensates, Phys. Rev. Lett. **99**, 190402 (2007).

[80] D. F. Walls and G. J. Milburn, *Quantum Optics*, 2nd ed. (Springer-Verlag, Berlin, 2008).

[81] R. Poldy, B. C. Buchler, P. A. Altin, N. P. Robins, and J. D. Close, Feasibility of squeezing measurements with cavity-based atom detection, Phys. Rev. A **86**, 043806 (2012).